Available online at www.sciencedirect.com

ScienceDirect

Advances in Space Research 75 (2025) 3427–3450

ADVANCES IN SPACE RESEARCH
(a COSPAR publication)

www.elsevier.com/locate/asr

Investigating the effects of different data classification methods on landslide susceptibility mapping

Halil Akinci *, Ayse Yavuz Ozalp

Artvin Çoruh University, Faculty of Engineering, Department of Geomatics Engineering, 08100 Artvin, Türkiye

Received 29 September 2024; received in revised form 26 November 2024; accepted 7 December 2024
Available online 12 December 2024

Abstract

In this study, landslide susceptibility maps (LSMs) were produced for three regions where landslides are common in the Eastern Black Sea Region of Türkiye. The regions studied include the districts of Trabzon, Rize and Artvin. The eXtreme Gradient Boosting (XGBoost) machine learning algorithm was used to generate the LSMs. Ten different factors that can affect landslides including lithology, land cover, topographic wetness index (TWI), plan and profile curvature, slope, elevation, aspect, distance to roads and drainages were used for the research. The study tested various spatial data classification methods for these factors. Specifically, the data was categorized using five distinct classification methods: "geometric interval," "equal interval," "manual interval," "natural breaks," and "quantile." The main objective of the study was to see how these classification methods affect the accuracy of LSMs. For this purpose, six different models using the XGBoost algorithm were created. In the first model, continuous data was used for most of the factors, while some factors (aspect, land cover and lithology) were used as discrete data. The other five models categorized the data using the different classification methods mentioned above. The receiver operating characteristic (ROC) curve and area under the curve (AUC) approach were used to measure how well each model performed. The results showed that the Model_1 using mostly continuous data performed the best among all three study areas with the highest AUC value. The model with the lowest AUC value was the model using the equal interval classification method (Model_3). The most important finding gained from this study was that when producing LSMs, it is preferable to maintain continuous data as is rather than reclassifying it, as this improves the accuracy of the susceptibility model.

Keywords: Landslide; Landslide susceptibility; Data classification methods; XGBoost

1. Introduction

Landslides are among the most common natural disasters worldwide. According to the World Bank, approximately 3.7 million square kilometers of land globally are at risk of landslides (Dilley et al., 2005). Additionally, it is anticipated that climate change will increase the frequency and intensity of heavy rainfall events, which are the primary triggers of landslides, thereby exacerbating the number of people exposed to landslide risk (Gariano and Guzzetti, 2016). Landslide losses can be reduced or even minimized by 90 %, according to Brabb (1993), provided that enough attention is given to identifying high-risk locations and researching triggering mechanisms. In this context, landslide susceptibility maps (LSMs) are important and powerful data for disaster avoidance, mitigating its effects and ensuring public safety as they indicate

* Corresponding author.
E-mail address: halil.akinci@artvin.edu.tr (H. Akinci).

https://doi.org/10.1016/j.asr.2024.12.020
0273-1177/

the landslide potential of a region (Shahzad et al., 2022; Tang et al., 2023; Zhou et al., 2024). Therefore, numerous landslide susceptibility (LS) mapping studies have been conducted around the world to identify landslide-prone areas and mitigate the potential negative impacts of landslides on human life, the environment and the economy.

Considering the aforementioned studies, traditional statistical models (such as logistic regression and frequency ratio) were used in the past to produce LSMs. More recently, machine learning (ML) and deep learning (DL) algorithms (Thi Ngo et al., 2021; Aslam et al., 2023; Padhan et al., 2023) have been used in tandem with advancements in information technologies. This has led to the production of high-precision and more reliable LSMs (Liu et al., 2023). According to Pradhan and Kim (2020), the main advantage of ML techniques is the ability to process high-dimensional, complex and non-linear data sets and thus be effective in solving the non-linear nature of geographic problems. In LS mapping, it has been observed that ensemble learning algorithms have recently come to the forefront and have been frequently preferred by researchers in a variety of tree-based ensemble learning algorithms such as Random Forest (RF) (Akinci, 2022; Sun et al., 2023a; Yu et al., 2023), Adaptive Boosting (AdaBoost) (Wu et al., 2020; Wei et al., 2022; Yu et al., 2023); Categorical Boosting (CatBoost) (Sahin, 2022; Ye et al., 2022; Usta et al., 2024), Light Gradient Boosting Machine (LightGBM) (Sahin, 2022; Song et al., 2023; Sun et al., 2023b) and eXtreme Gradient Boosting (XGBoost) (Kavzoglu and Teke, 2022; Sun et al., 2023b; Zhang et al., 2023). However, there seems to be no consensus in the literature on which model is most suitable for LS mapping (Hong et al., 2016; Aditian et al., 2018; Shahzad et al., 2022).

Although the number of groups can be further increased, artificial intelligence-based LS mapping studies conducted worldwide can be generally classified into seven groups: (i) studies using a single ML or DL algorithm (Mutlu et al., 2019; Can et al., 2021; Zhang et al., 2023), (ii) studies comparing the performance of different ML or DL algorithms (Cao et al., 2020; Thi Ngo et al., 2021; Ajim Ali et al., 2022), (iii) studies investigating the effects of different training/test ratios (such as 50:50, 60:40, 70:30, and 80:20) on model performances (Saha et al., 2021; Nurwatik et al., 2022; Xu et al., 2024), (iv) studies investigating the impact of different presence-absence or landslide/non-landslide ratios (such as 1:1, 1:2, 1:4, 1:8, and others) on the performance of ML models (Pourghasemi et al., 2020; Tang et al., 2023), (v) studies investigating the effects of non-landslide sample selection strategies on landslide susceptibility mapping (Ye et al., 2023; Gu et al., 2024; Zhou et al., 2024), (vi) studies evaluating the impact of varied sample resolution and spatial resolution on LS mapping results (Yu and Chen, 2024), (vii) spatial comparison and accuracy assessment of LSMs produced by reclassifying landslide susceptibility indices (LSI) using different data classification algorithms (such as "natural breaks, equal interval, quantile and standard deviation") (Baeza et al., 2016; Zhao and Chen, 2020; Barman and Das, 2024). For example, Nurwatik et al. (2022) used three ML algorithms including RF, Naïve Bayes (NB), and k-Nearest Neighbor (KNN) and 12 conditioning factors in their LS mapping study in Malang Regency, Indonesia. Using 50:50, 60:40 and 70:30 ratios for the separation of training and test data sets, the researchers found that the model with a 70:30 ratio performed best in the RF algorithm. Tang et al. (2023) investigated the effect of five different landslide/non-landslide sampling sets (1:1, 1:2, 1:4, 1:8, and 1:16) in their LS mapping study using C5.0, Logistic Regression (LR), Support Vector Machine (SVM), and Convolution Neural Network (CNN) algorithms. The researchers determined that CNN, SVM and LR models performed better at a 1:2 sample ratio than at a 1:1 sample set. Whereas, Zhou et al. (2024) used six ML algorithms in their research, in which they aimed to increase the accuracy of LS models by extracting high quality non-landslide samples. Conducted in the Zigui-Badong section of the Three Gorges Reservoir area (TGRA) in China, the researchers first produced a LSM of the study area with the LR model and then selected the non-landslide samples from the areas with low susceptibility class. In the studies conducted by Baeza et al. (2016) in Spain and by Üzel Günini and Öztürk (2021) in Türkiye at different times, LSMs were produced using different data classification methods (such as natural breaks, equal interval, geometric interval, quantile and standard deviation). Based on accuracy assessments, the researchers concluded that the method of natural breaks was the most appropriate classification technique for modeling LS in the study areas. However, Barman and Das (2024) compared four classification methods (geometric interval, natural breaks, quantile interval, and mean-standard deviation) in their LS study in the Aizawl region of northeast India and concluded that the mean-standard deviation classification method was the best methodology for mapping LS in the study area.

In the production of LSMs, in addition to the landslide inventory, many conditioning factors need to be considered together. Identifying the conditioning factors is the most crucial step in the modeling procedure. The success or failure of a susceptibility model largely depends on the selection and accuracy of conditioning factors, algorithm selection, study scale, sampling strategies, analysis processes and data splitting rates (Pourghasemi et al., 2020; Abraham et al., 2021; Liu et al., 2023). Singh et al. (2023) reported that the diversity of conditioning factors significantly affects LSMs and their accuracy. Conditioning factors, by their nature, are represented by either discrete (such as lithology, land cover and aspect) or continuous data (such as elevation, slope, curvature, topographic wetness index, distance to roads). However, in the modeling phase, usually all raster-based factor data are reclassified into a discrete structure. At this stage, it is seen that the uncertainty about which ML model is the most appropriate for LSM also arises for conditioning factors. In other words, it is often left to the discretion of the researcher to decide which conditioning factors are most suitable for LSM, which classification method (such as equal interval, geometric interval, natural breaks, and quantile) is most suitable for reclassifying the conditioning factors, or what the number of classes should be in the reclassification, even though it is certain for aspect and curvature. For example, if we consider the slope factor, we see that some researchers categorize slope into four subclasses (Xu et al., 2024), while others have five (Vega et al., 2023; Zhou et al., 2024), six (Dou et al., 2023; Xiong et al., 2023), seven (Gu et al., 2024), eight (Sahin, 2022; Chang et al., 2023; Yao et al., 2023), nine (Sun et al., 2023a) or ten subclasses (Kilicoglu, 2021; Akinci, 2022; Yavuz Ozalp et al., 2023). Again, we see that some researchers prefer equal interval (Zhang et al., 2022; Sun et al., 2023a; Yavuz Ozalp et al., 2023), while others prefer natural breaks (Sahin and Colkesen, 2021; Kavzoglu and Teke, 2022; Yao et al., 2023) classification method in the formation of subclasses. In some studies, the slope was manually reclassified according to the preferences of the researchers (Wang et al., 2020; Vega et al., 2023). Youssef and Pourghasemi (2021), on the other hand, didn't reclassify the slope and preferred to use it as continuous data.

Considering the literature summary above, it is seen that there is a lack of studies investigating the effects of the procedures utilized in the reclassification of conditioning factors, which have an important role in the generation of LSMs, on the susceptibility model's performance. Therefore, the purpose of this study was to look at the effects of reclassifying conditioning factors using various classification methods on the performance of ML models. This is the novel component of the research that will add to the body of knowledge. For this purpose, LSMs were produced using XGBoost algorithm in three different study areas covering Trabzon, Rize, and Artvin districts. In this study, XGBoost algorithm was also preferred as it has shown superior performance compared to other ML algorithms in different susceptibility mapping applications such as landslide, flood, forest fire and gully erosion (Alkan Akıncı and Akıncı, 2023; Dawson et al., 2023; Bammou et al., 2024). Considering that the results obtained from a single study area may be insufficient to make a generalization, the LS mapping studies were carried out in three distinct locations. In the study, aspect, distance to drainages, distance to roads, elevation, land cover, lithology, plan curvature, profile curvature, slope and topographic wetness index (TWI) were used as conditioning factors. Five different classification methods (natural breaks, manual, quantile, equal interval and geometric interval) were applied to reclassify the spatial data of conditioning factors. Using the XGBoost method, six distinct susceptibility models were created for the study, and the models' performances were assessed.

2. Material and methods

This study's primary goal is to determine how classification techniques affect the ML model's performance when used to prepare spatial data set of conditioning factors. The study generally includes eight steps: (1) collecting basic spatial data (such as topographic maps, geological maps, roads and land cover data) from relevant public institutions or data sources, (2) producing Digital Elevation Models (DEMs) of the study areas, (3) obtaining discrete (such as aspect) and continuous factor data (such as elevation, plan/profile curvature, TWI) from DEM, (4) reclassifying continuous factors using natural breaks, manual, quantile, equal interval and geometric interval classification methods in order to produce raster datasets, (5) collecting landslide inventory data and creating training and validation datasets, (6) testing the independence of conditioning factors using multicollinearity analysis, (7) generating LSMs of study areas using the XGBoost algorithm, (8) evaluating the models' performance by utilizing the receiver operating characteristic (ROC) curve and area under the curve (AUC). Fig. 1 displays the process diagram that illustrates the methods employed in this investigation.

In the study, six different susceptibility models using the XGBoost algorithm were developed. Due to their nature, aspect, land cover and lithology are used as discrete data in all models. In Model_1, distance to drainages, distance to roads, elevation, plan curvature, profile curvature, slope and TWI were used as continuous data without reclassification. Distance to drainages, distance to roads, elevation, slope and TWI were reclassified into nine subclasses using natural breaks in Model_2, equal interval in Model_3, manual interval in Model_4, quantile in Model_5 and geometric interval in Model_6. Plan and profile curvature were divided into 3 subclasses (concave, flat, convex) and given as input to other models except Model_1. The following software and libraries were used to conduct this study: ArcGIS 10.5, SAGA GIS 9.0.1, QGIS 3.36.2, RStudio 2023.12.1, and caret library (Kuhn, 2008).

2.1. Study areas

The northern parts of Türkiye are severely affected by floods and landslides. The Black Sea Region of Türkiye is the most prone to landslides, as is commonly known (Duman and Çan, 2023). According to the natural disaster statistics report of the Disaster and Emergency Management Presidency (DEMP), 1517 landslides occurred in Trabzon, 1319 in Rize, 913 in Giresun and 765 in Artvin, which are provinces in the Eastern Black Sea Region. Landslides in Trabzon, Rize and Artvin account for approximately 16 % of 23,041 landslides that have occurred in Türkiye since 1950 (DEMP, 2018). Therefore, in this study, Ortahisar, Yomra and Arsin districts of Trabzon, Ardeşen and Fındıklı districts of Rize, Hopa and Kemalpaşa districts of Artvin were selected as study areas.

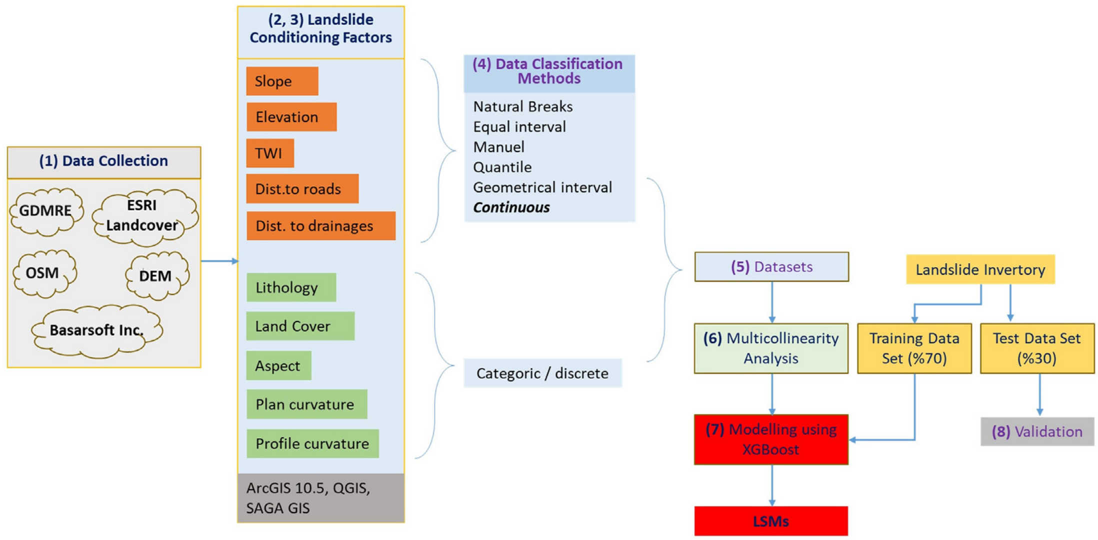

Fig. 1. Landslide susceptibility modelling workflow diagram.

2.1.1. Hopa and Kemalpaşa

Hopa and Kemalpaşa are two of Artvin's three districts that border the Black Sea. The study area covering these two districts with a surface area of 187.63 km^2 lies geographically between 41°19′5.85″–41°31′15.27″ north latitude and 41°20′14.4″–41°37′14.98″ east longitude (Fig. 2). The elevation ranges from 0 to 1860 m, and the slope varies from 0 to 70.82°in the study area. About 75 % of the research area, which is primarily composed of very steep topography, has a slope angle greater than 20°.

Considering the meteorological observation values for the study area for the years 1991–2021, it is seen that the monthly average temperature is 13.1 °C and the total annual precipitation is 2435 mm. The highest average temperature in the study area is 23.3 °C in August and the lowest average temperature is 2.3 °C in February (ClimateData, 2024). According to the Thornthwaite climate classification (1948), the study area is classified as "A,B′2,r,b′4" (A: very humid, B′2: 2. degree mesothermal, r: no or very little water deficit, b′4: summer evaporation rate 49.6 %) climate class (GDM, 2024a).

According to the CORINE 2018 land cover dataset (CLMS, 2020), 64.35 % of the study area is forest, 31.29 % is agriculture, 3.62 % is artificial surfaces (such as discontinuous urban fabric, etc.), while the rest is covered by transitional woodland/shrub.

The research area is divided into 14 lithological units based on the geological map that was provided by the General Directorate of Mineral Research and Exploration (GDMRE). Table 1 provides descriptive data regarding the lithological units.

2.1.2. Ardeşen and Fındıklı

The second study area in this study is the districts of Ardeşen and Fındıklı in Rize province. The surface area of the study area, where the altitude varies between 0 and 3497.38 m, is 760.012 km^2. The study area is geographically located between 40°57′37.42″–41°19′37.57″ north latitude and 40°57′41.5″–41°23′44.21″ east longitude (Fig. 3). The research region exhibits an average slope of 28 degrees, with a range of slopes between 0 and 75.82 degrees. Approximately 80 % of this study area has slopes above 20°. Only 3.37 % of the study area consists of flat or almost level terrain with slopes below 5 degrees.

In Rize, which has a cool climate in summer, mild in winter and rainy in all seasons, average temperatures vary between 6.8 °C and 23.3 °C. According to the General Directorate of Meteorology's (GDM) measuring data for the years 1928–2023, the lowest average temperature in Rize is 3.7 °C in February and the highest is 26.6 °C in August. The average annual total precipitation in Rize was 2300 mm (GDM, 2024b). As in the first study area covering Hopa and Kemalpaşa districts, in Ardeşen and Fındıklı, according to the Thornthwaite climate classification (1948), their climate class are "A,B′2,r,b′4" (A: very humid, B′2: 2. degree mesothermal, r: no or very little water deficit, b'4: summer evaporation rate 50.4 %) (GDM, 2024c).

Based on the CORINE 2018 land cover dataset (CLMS, 2020), the study area consists of 59.27 % forest, 21.12 % agriculture, approximately 1 % artificial surfaces (such as urban fabric, roads, railways, etc.), 8.07 % natural grassland, and the remaining 10.54 % transitional woodland/shrub, bare rock, patchily vegetated areas, and water courses.

According to the geological map obtained from the GDMRE, there are 9 lithological units in the study area. Descriptive information about the lithological units is given in Table 2.

2.1.3. Ortahisar, Yomra and Arsin

The third study area, covering Ortahisar, Yomra and Arsin districts of Trabzon, is located between 40°42′33.54″–41°0′48.04″ north latitude and 39°36′27.69″–40°0′23.45″

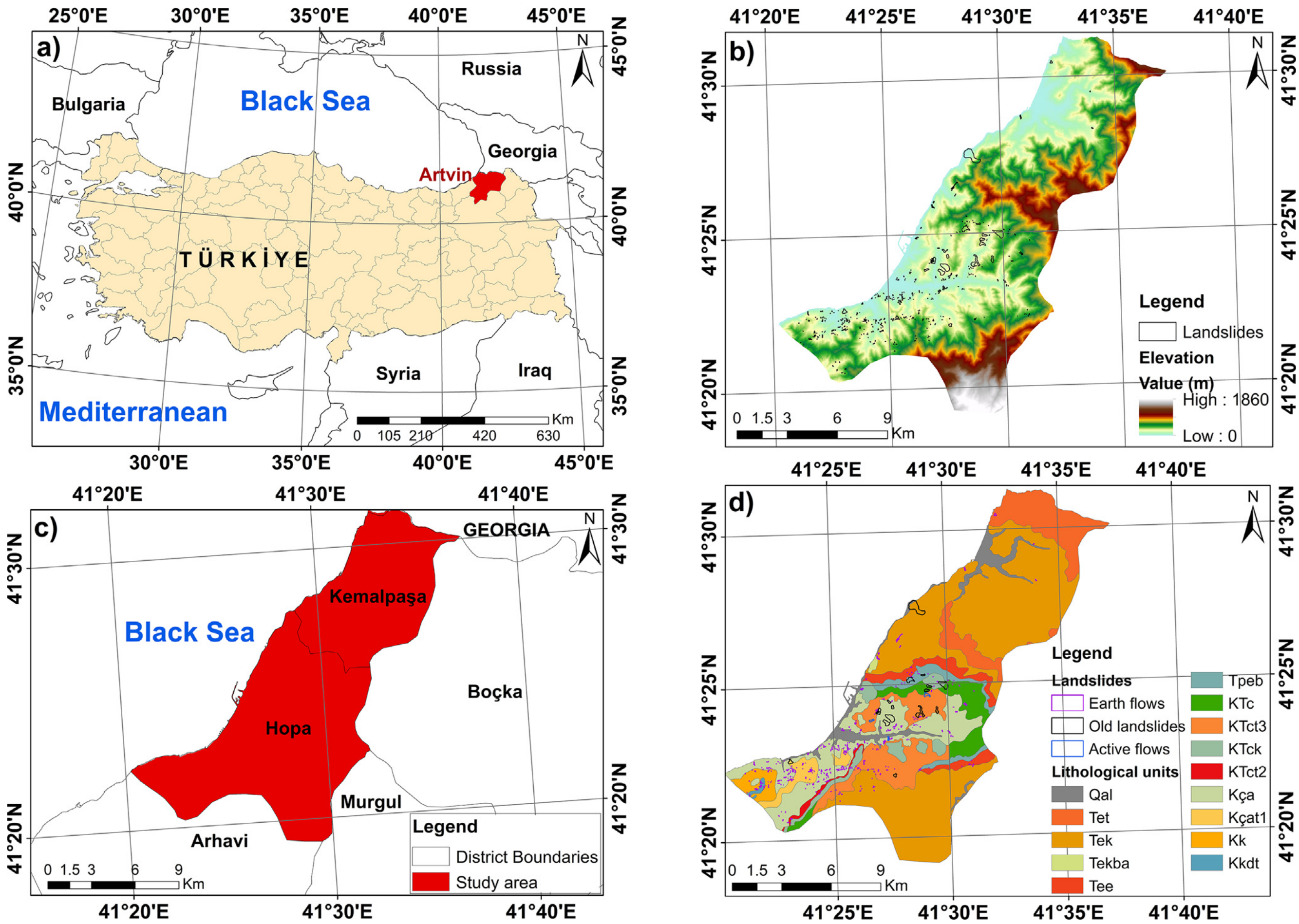

Fig. 2. (a) Location of Artvin in Turkey, (b) Elevation map of the study area, (c) Districts of Artvin and the study area, (d) Lithology map of the study area.

Table 1
Lithological units in Hopa and Kemalpaşa (Keskin, 2013).

No	Symbol	Formation Name	Age	Content of Formation
1	Qal	–	Quaternary	Alluvium
2	Tet	Taşpınar Frm.	Middle Eocene	It consists of andesitic and dacitic volcanics and volcano-clastic rocks
3	Tek	Kabaköy Frm.	Middle Eocene	It consists of andesitic, basaltic lava and pyroclastics, conglomerate, sandy limestone, sandstone, marl and tuffs
4	Tekba	–	Middle Eocene	Basalt, Andesite
5	Tee	Erenler Frm.	Middle Eocene	It consists of an alternation of mudstone, claystone and sandstone
6	Tpeb	Bakırköy Frm.	Paleocene-Early Eocene	It consists of siltstone, claystone, sandstone conglomerate, clayey-sandy limestone and marl
7	KTc	Cankurtaran Frm.	Maastrichtian-Danian	It consists of sandy limestone, micritic limestone and clastic rocks
8	KTct3	–	Maastrichtian-Danian	Tuff, marl, limestone, volcanic sandstone, agglomerate
9	KTck	–	Maastrichtian-Danian	Gray and red colored limestone
10	KTct2	–	Maastrichtian-Danian	Tuff, marl, fine-grained agglomerate
11	Kça	Çağlayan Frm.	Campanian-Maastrichtian	It consists of basaltic, andesitic lava and pyroclastics, mudstone, sandstone and tuffs
12	Kçat1	–	Campanian-Maastrichtian	Clayey tuff, tuffaceous sandstone, sandy limestone and breccia
13	Kk	Kızılkaya Frm.	Santonian	It consists of dacite, rhyolite, rhyodacitic lava and pyroclastics
14	Kkdt	–	Santonian	Dacitic lava-tuff

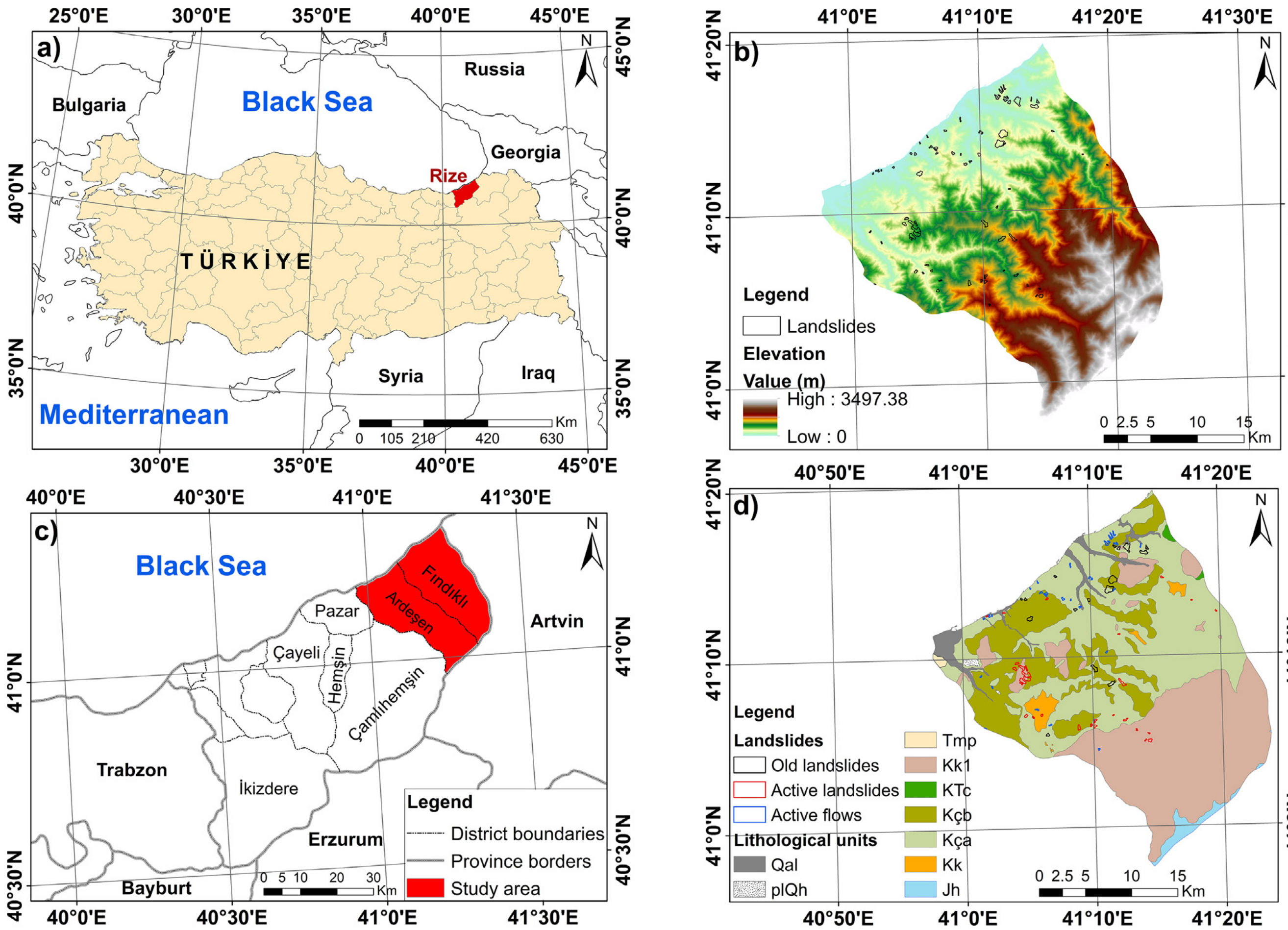

Fig. 3. (a) Location of Rize in Turkey, (b) Elevation map of the study area, (c) Districts of Rize and the study area, (d) Lithology map of the study area.

Table 2
Lithological units in Ardeşen and Fındıklı (Keskin, 2013).

No	Symbol	Formation Name	Age	Content of Formation
1	Qal	–	Quaternary	Alluvium
2	plQh	Hamidiye Frm.	Plio-Quaternary	It consists of terrestrial conglomerate with sand and clay lenses
3	Tmp	Pazar Frm.	Early-Middle Miocene	It consists of an alternation of sandstone, marl, conglomerate and claystone
4	Kk1	Kaçkar Granitoid-I	Campanian-Maastrichtian	Granite and granodiorite, quartz monzonite, quartz diorite, syenite, monzonite, microsyenite
5	KTc	Cankurtaran Frm.	Maastrichtian-Danian	It consists of sandy limestone, micritic limestone and clastic rocks
6	Kçb	Çayırbağı Frm.	Maastrihtiyen	It consists of rhyolite, rhyodacite and dacitic lava and pyroclastics
7	Kça	Çağlayan Frm.	Campanian-Maastrichtian	It consists of basaltic, andesitic lava and pyroclastics, mudstone, sandstone and tuffs
8	Kk	Kızılkaya Frm.	Santonian	It consists of dacite, rhyolite, rhyodacitic lava and pyroclastics
9	Jh	Hamurkesen Frm.	Early Jurassic (Liassic)	It consists of basaltic, andesitic, dacitic lava and pyroclastics, sandstone, marl, red limestone and shale

east longitude and has a total area of 593.14 km^2 (Fig. 4). Within the scope of the research, the slope ranges from 0 to 73.38 degrees and the elevation from 0 to 2305 m. Similar to the preceding two regions, this research area, encompassing three districts of Trabzon, exhibits a challenging topography. Approximately 66 % of the study area has slopes above 20°.

In Trabzon, where two different climate types are seen, a warm and rainy climate type is common in the coastal areas with the effect of the sea, while the continental climate is dominant in the inland areas. According to the measurement data of the GDM for the years 1927–2023, the coldest average temperature in Trabzon at 4.4 °C in February and the warmest average temperature at 26.6 °

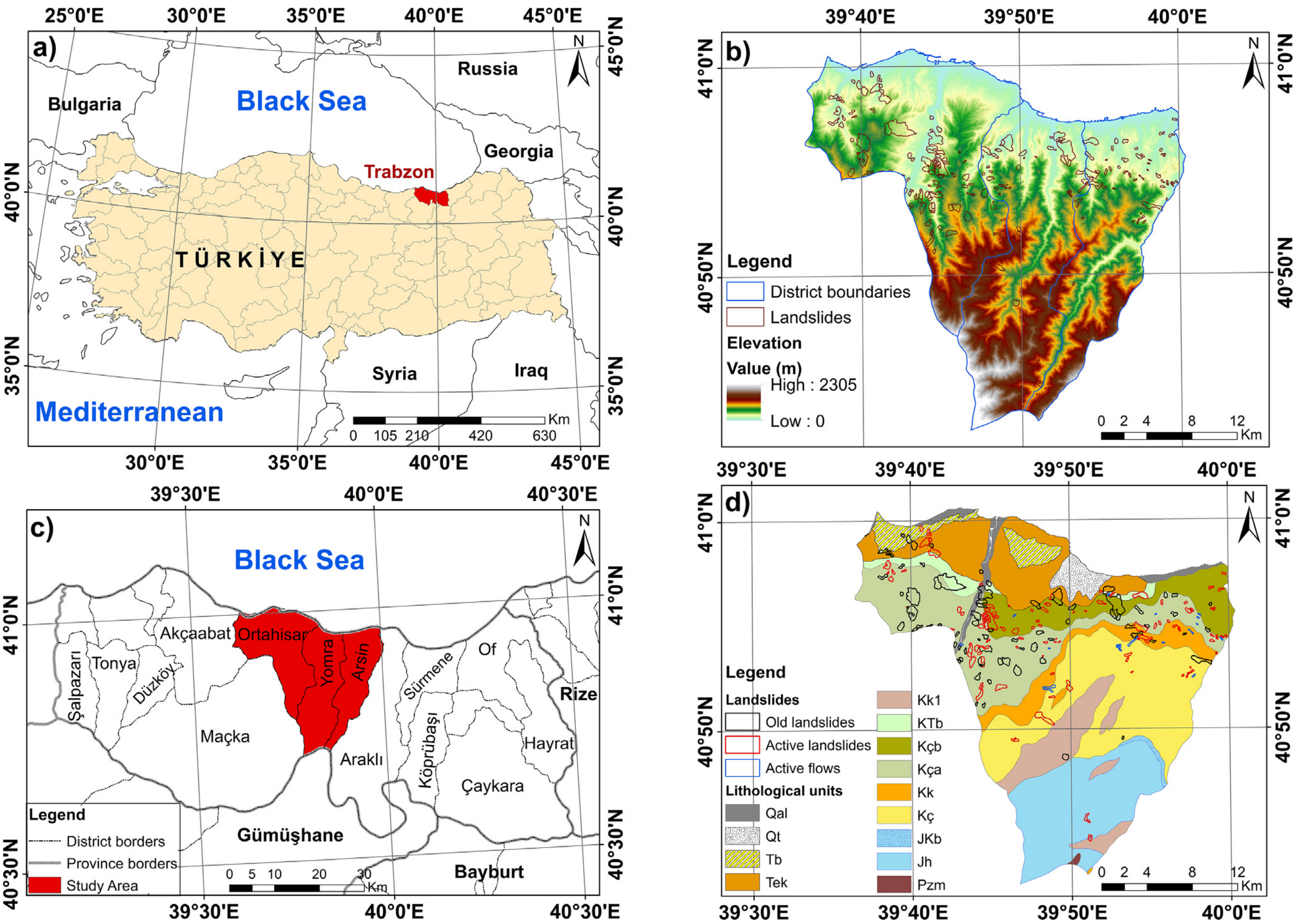

Fig. 4. (a) Location of Trabzon in Turkey, (b) Elevation map of the study area, (c) Districts of Trabzon and the study area, (d) Lithology map of the study area.

C in August. The mean annual precipitation was calculated to be 828.9 mm (GDM, 2024d). According to the Thornthwaite climate classification (1948), Trabzon has a semi-humid, 2nd degree mesothermal climate type (C2, B′2,s,b′4) with a summer evaporation rate of 49.8 % and moderate water deficit in summer (GDM, 2024e).

Based on the CORINE 2018 land cover dataset (CLMS, 2020), the study area consists of 32.4 % forest, 58.58 % agriculture, 5.95 % artificial surfaces (such as urban fabric, industrial areas, transportation units etc.), and the rest is comprised of natural grassland and transitional woodland/shrub.

The study area is divided into 13 lithological units based on the 1/100.000 scale geological map that was obtained from the GDMRE. Table 3 contains descriptive information about the lithological units.

2.2. Landslide conditioning factors

The topography, geology, and geoenvironmental features of the region, as well as data from landslide inventories, are the primary inputs used to create LSMs. However, it is important to note that there is no universally accepted criterion in the existing literature for selecting conditioning factors. Furthermore, a factor that proves to be significant in one study area may not hold the same importance in another (Demirağ Turan et al., 2020; Akinci et al., 2020). Therefore, the specific characteristics of the study area and the data at hand play a crucial role in identifying the conditioning factors.

In the bibliometric analysis conducted by Liu et al. (2022), covering the years 1999–2021, 4732 articles published in Web of Science were analyzed and it was determined that the most commonly used factors in LS mapping studies were slope, aspect, lithology, elevation, distance from river, distance from faults, land use/land cover, distance to roads, precipitation, TWI, plan curvature and profile curvature. In this context, susceptibility assessments were carried out using ten conditioning factors (lithology, elevation, land cover, aspect, slope, plan and profile curvatures, topographic wetness index (TWI), distance to drainages, distance to roads) taking into account the geoenvironmental characteristics of three regions with similar topographic characteristics. In this study, ten of the twelve conditioning factors identified by Liu et al. (2022) were used, while two factors (precipitation and dis-

Table 3
Lithological units in Ortahisar, Yomra and Arsin (Güven, 1998; Keskin, 2013).

No	Symbol	Formation Name	Age	Content of Formation
1	Qal	–	Quaternary	Alluvium
2	Qt	–	Quaternary	Terrace: conglomerate, sand, clay
3	Tb	Beşirli Frm.	Pliocene	Sandstone, mudstone, conglomerate, basalt, agglomerate
4	Tek	Kabaköy Frm.	Middle Eocene	It consists of andesitic, basaltic lava and pyroclastics, conglomerate, sandy limestone, sandstone, marl and tuffs
5	Kk1	Kaçkar Granitoid-I	Campanian-Maastrichtian	Granite and granodiorite, quartz monzonite, quartz diorite, syenite, monzonite, microsyenite
6	KTb	Bakırköy Frm	Paleocene-Early Eocene	It consists of siltstone, claystone, sandstone conglomerate, clayey-sandy limestone and marl
7	Kçb	Çayırbağı Frm.	Maastrichtian	It consists of rhyolite, rhyodacite and dacitic lava and pyroclastics
8	Kça	Çağlayan Frm.	Campanian-Maastrichtian	It consists of basaltic, andesitic lava and pyroclastics, mudstone, sandstone and tuffs
9	Kk	Kızılkaya Frm.	Santonian	It consists of dacite, rhyolite, rhyodacitic lava and pyroclastics
10	Kç	Çatak Frm.	Turonian-Coniacian	It consists of basalt, andesitic lava and pyroclastics, clayey limestone, marl, siltstone and claystone
11	JKb	Berdiga Frm.	Late Jurassic-Early Cretaceous	It consists of clayey limestone, cherty limestone and sandy limestone
12	Jh	Hamurkesen Frm.	Early Jurassic (Liassic)	It consists of basaltic, andesitic, dacitic lava and pyroclastics, sandstone, marl, red limestone and shale
13	Pzm	Metamorphic Basement	Paleozoic	Gneiss, mica schist, quartz-chlorite schist

tance from faults) were left out. Since there is no active fault near the study areas and there is no tectonic activity in the region, the distance from faults factor was not preferred in the study. Additionally, the precipitation element was disregarded because a comprehensive precipitation distribution map could not be generated due to the inadequate number of meteorological stations in the study areas.

Digital topographic maps at a scale of 1/25.000 for study areas were obtained from the General Directorate of Mapping. Using contour lines on the maps, TIN (Triangulated Irregular Network) data of the study areas were generated in ArcGIS 10.5 software, and DEMs were acquired with a spatial resolution of 10 m via the "TIN to Raster" function. The data for elevation, slope, aspect, plan curvature, profile curvature, and TWI were obtained via the "3D Analyst Tools" functions of the ArcGIS software. Utilizing the "Basic Terrain Analysis" function of SAGA GIS 9.0.1 software, the drainage networks of the research regions were constructed from the DEM. For the study regions, the GDMRE provided digital geological maps with a scale of 1/100.000. And using these maps, lithology maps were made. In addition, the land cover data with a resolution of 10 m for the research areas were acquired from ESRI. On the other hand, Artvin Regional Directorate of Forestry provided digital road network data for the Hopa and Kemalpaşa districts, while Başarsoft provided data for the Ardeşen and Fındıklı districts. The road data for Trabzon's districts was acquired from OpenStreetMap using the GIS software's "QuickOSM" plugin. The "Euclidean Distance" function of ArcGIS 10.5 software was utilized to generate factor maps for the study areas, namely for distance to roads and distance to drainages.

There are a lot of studies (Kavzoglu et al., 2014; Youssef and Pourghasemi, 2021; Ye et al., 2022) that describe the relationship between the criteria that were chosen and the occurrence of landslides. For this reason, in this study, it was deemed appropriate to present only the data sources and descriptive information for conditioning factors (Table 4).

2.3. Preparation of conditioning factor maps using data classification methods

Data classification is the process of grouping continuous data into classes at certain intervals and thus making it simpler and more understandable (Üzel Günini and Öztürk, 2021). Classification involves a different redistribution of information depending on the different methods applied to the data (Baeza et al., 2016). "Data discretization" is another term for this process, which is described as the conversion of continuous values into a set of intervals (Zhao and Chen, 2023). Various classification methods have been developed to categorize continuous data. The classification methods included in ESRI ArcGIS software and widely used in cartography are manual, equal interval, defined interval, quantile, natural breaks, geometrical interval and standard deviation. Two parameters are usually used to describe classification methods. These are the number of classes and class intervals (Li and Shan, 2022). Class intervals vary according to the classification method used. Table 5 provides descriptive information on the classification methods utilized in this investigation.

In this study, the spatial datasets for conditioning factors were reclassified with five classification methods (manual, equal interval, natural breaks, quantile and

Table 4
Sources and characteristics of the spatial data used in the study.

Data	Source	Scale/resolution (m)	Purpose of use
DEM	GDM	10 m	To extract topographic factors such as elevation, slope, aspect, curvature, TWI, etc.
Geological maps	GDMRE	1:100,000	To extract lithology
Landslide inventory	GDMRE	1:25,000	To extract landslide information
Land cover	ESRI	10 m	Land cover
Roads	Artvin RDF	10 m	To produce the 'distance to roads" maps
	Başarsoft Inc.	10 m	
	OpenStreetMap	10 m	

Table 5
Data classification methods and descriptions.

Classification methods	Description
Manual classification	The user or analyst determines the number of classes and their ranges (de Smith et al., 2018)
Quantile	Each predetermined number of classes contains an equal number of observations or features (Longley et al., 2005). Quantile classification works effectively for linearly distributed data (ESRI, 2024a)
Equal interval	The data are divided into equal-sized classes (0–100, 100–200, 200–300, etc.). The number of classes to provide is up to the user (Campbell and Shin, 2012; ESRI, 2024a)
Geometric interval	This classification technique uses geometric series to define class intervals, resulting in class breaks. The procedure minimizes the sum of squares of the number of elements in each class, ensuring that each class range has nearly the same amount of values in each class and that the change between intervals is relatively consistent (ESRI, 2024a)
Natural breaks (Jenks)	Classes are determined based on the natural groups inherent in the data. Class ranges are created to best combine similar values and maximize differences between classes (ESRI, 2024a)

geometrical interval) offered by ArcGIS software. Since the number of classes is determined automatically in standard deviation and defined interval methods, they were not used in this study. In order to be consistent with the number of classes in the aspect layer, conditioning factors with continuous values such as elevation, slope, TWI, distance to drainages and distance to roads were divided into nine subcategories (Annex Tables 1–3).tpb 3

2.4. Preparation of training and validation datasets using landslide inventory data

Landslide inventory maps (LIMs) used in the training and testing phase for ML models are the fundamental maps showing the spatial distribution and characteristics of landslides that have happened in previous years (Duman and Çan, 2023). These maps are usually produced by interpretation of aerial photographs and high-resolution satellite imagery and data obtained as a result of on-the-ground field investigations. Nowadays, it is seen that deep learning algorithms such as Convolutional Neural Networks (CNNs), Fully Convolutional Networks (FCNs) and ResU-NET and self-supervised learning (SSL) models come to the forefront in the detection of landslides for the production of accurate LIMs (Ghorbanzadeh et al., 2022, 2023, 2024). LIMs are an important dataset needed for susceptibility models to explain the correlation between previous landslides and factors that contribute to their occurrence (Chen et al., 2018). The GDMRE provided the digital LIMs on a 1/25.000 scale for this investigation. The LIM of the first study area covering Hopa and Kemalpaşa districts was updated with landslide locations obtained from Artvin Provincial Directorate of Disaster and Emergency.

There are 490 landslide polygons in the study area covering Hopa and Kemalpaşa districts. Of these, 19 were obtained from the GDMRE and the remaining 471 were obtained from Artvin Provincial Directorate of Disaster and Emergency. Of the 19 landslides obtained from the GDMRE, 16 are old landslides and three are of active flow type. Approximately 99 % of the landslides obtained from Artvin Provincial Directorate of Disaster and Emergency are landslides triggered by the heavy rains experienced in the region on August 24, 2015. Of these landslides, 430 were earth flow, one was rotational slide, three were translational slide, six were creep and 24 were complex. The landslides range in length from 6 to 393 m and in width from 4 to 290 m. With a spatial resolution of 10 m, 16,924 pixels are used to depict the landslide polygons in the research region.

There are 76 landslide polygons in the area covering Ardeşen and Fındıklı districts. GDMRE classified 16 of these landslides as old landslides, 30 as active landslides and 30 as active flows. With a total area of 621.06 ha, the landslide polygons cover 0.82 % of the study area. The areas of landslide polygons vary between 0.74 ha and 54.67 ha. According to the classification of Varnes (1978), the landslides in the study area are mostly flow and rotational slide types (Yavuz Ozalp et al., 2023). At a spatial resolution of 10 m, the landslide polygons within the study area are represented by 62,089 pixels.

In the third study area covering Ortahisar, Yomra, and Arsin districts, there are 213 landslide polygons. Of these, 75 were classified as old landslides, 119 as active landslides and 19 as active flows. The landslide polygons have a total area of 3026.75 ha and their areas vary between 0.6 ha and 204.74 ha. The landslide polygons cover 5.10 % of the study area. Yalcin et al. (2011) reported that landslides caused by heavy rainfalls in Trabzon mostly exhibited shallow translational features. The research field has 302,699 pixels that represent the landslide polygons. These pixels have a spatial accuracy of 10 m.

ML-based landslide susceptibility models need positive landslide examples as well as negative landslide examples in the training phase. For this reason, with a code written in R programming language, 16,924 non-landslide samples were randomly selected in Hopa and Kemalpaşa, 62,089 in Ardeşen and Fındıklı, and 302,669 in Ortahisar, Yomra and Arsin, respectively. For each study area, the overall dataset including landslide and non-landslide samples was divided 70:30 to obtain training and validation datasets.

2.5. Extreme Gradient Boosting (XGBoost)

The XGBoost algorithm, which is used in regression and classification problems, was first introduced by Chen and Guestrin (2016). The XGBoost algorithm is an optimized version of GBM (Gradient Boosting Machine) that use a gradient boosting framework and decision tree-based ensemble learning. It is designed to achieve faster and more accurate predictions (Kurt et al., 2020; Can et al., 2021; Kavzoglu and Teke, 2022). The XGBoost algorithm has numerous advantages, particularly in terms of computational speed and regularization, which are not present in the Gradient Boosting Machines technique. These advantages primarily enhance the efficiency of the model (Kurt et al., 2020; Jennifer, 2022). XGBoost is seen as an advantageous method due to its high prediction power, its ability to prevent overfitting, its ability to manage empty data and its speed (Yeşilyurt and Dalkılıç 2021; Jennifer 2022). The working principle of XGBoost is as follows: an initial prediction is made for a training dataset using XGBoost. Residuals are calculated by subtracting the predicted values from the observed ones. A decision tree is then constructed that predicts the residuals and a similarity and gain score is calculated for the tree. The output of the first tree is calculated and this output becomes the new residual for the dataset used to build another tree. Each subsequent tree learns from the residuals of the previous trees. This process is repeated until the residuals stop decreasing or until a set number of trees is reached (ESRI, 2024b). In this study, XGBoost was implemented using the "xgbTree" method of the "caret" library with the default hyperparameter settings (Kuhn, 2008).

3. Results

3.1. Multicollinearity analysis

Multicollinearity is one of the serious problems that need to be solved before starting modelling the data. Multicollinearity occurs when there exists a correlation between two or more independent variables (explanatory variables) in a regression model. Even a little bit of multicollinearity can sometimes cause big problems (Daoud, 2017; Kim, 2019). The multicollinearity problem causes misleading findings by decreasing the model's prediction accuracy, reducing the statistical significance of independent variables and thus misinterpreting the model results (Kim, 2019; Chen and Chen, 2021; Kavzoglu and Teke, 2022).

As in all regression analysis studies, it is important to verify the independence of variables from each other in ML-based landslide susceptibility mapping studies, and in this context, the selection of proper variables is carried out by multicollinearity analysis (Chen et al., 2018; Aslam et al., 2023). Variance inflation factors (VIF) and tolerance (TOL) are commonly employed statistical measures for detecting multicollinearity, as acknowledged by several studies (Pourghasemi et al., 2018; Nohani et al., 2019; Akinci and Yavuz Ozalp, 2021). VIF represents the rise in a regression coefficient's variance brought on by multicollinearity. TOL, the inverse of VIF value, quantifies the extent to which an independent variable's volatility is not accounted for by other independent variables. Tolerance values below 0.10 indicate the presence of

Table 6
Results of the multicollinearity analysis.

Conditioning factors	Hopa – Kemalpaşa		Ardeşen – Fındıklı		Ortahisar-Yomra-Arsin	
	VIF	TOL	VIF	TOL	VIF	TOL
Aspect	1.02017	0.98023	1.03193	0.96906	1.02729	0.97343
Distance to drainages	1.16519	0.85823	1.09264	0.91521	1.08649	0.92039
Distance to roads	1.18981	0.84047	1.82322	0.54848	1.20709	0.82844
Elevation	1.28921	0.77567	1.94278	0.51473	1.33657	0.74818
Land cover	1.19038	0.84007	1.05574	0.94720	1.22575	0.81583
Lithology	1.11089	0.90018	1.09879	0.91009	1.10073	0.90849
Plan curvature	1.29729	0.77084	1.27513	0.78423	1.23661	0.80866
Profile curvature	1.12794	0.88657	1.10272	0.90685	1.09855	0.91029
Slope	1.38187	0.72366	1.41664	0.70589	1.47861	0.67631
TWI	1.42129	0.70359	1.59474	0.62706	1.44794	0.69064

multicollinearity. Variables with VIF exceeding 10 or TOL below 0.1 are multicollinear and should be omitted from the model (Wang et al., 2019; Hong et al., 2020; Wei et al., 2022).

Table 6 displays multicollinearity analysis results for all three research regions. Since the VIF values were below 10 and the TOL values were over 0.1 in all three research areas, it can be inferred that there was no multicollinearity among the conditioning factors. Consequently, the susceptibility model encompassed all factors.

Pearson correlation coefficient method was also used to test the correlation between conditioning factors. A correlation coefficient ranging between −1 and +1, where 0 indicates that there is no correlation between the factors. A correlation coefficient of +1 indicates a positive correlation between the factors, while a correlation coefficient of −1 indicates a negative correlation. On the other hand, a correlation coefficient greater than 0.7 indicates a high correlation between the two conditioning factors and that one of the factors should be removed from the model (Kalantar et al., 2020; Putriani et al., 2023; Huang and Chen, 2024). Correlation matrices showing the Pearson's correlation coefficients between conditioning factors are given in Fig. 5. Correlation coefficients vary between −0.38 and 0.33 for Hopa-Kemalpaşa study area (Fig. 5a), between −0.41 and 0.46 for Ardeşen-Fındıklı study area (Fig. 5b), and between −0.43 and 0.45 for Ortahisar, Yomra, Arsin study area (Fig. 5c). These coefficients indicate that there is not a strong correlation between the factors.

3.2. Landslide susceptibility mapping

The XGBoost method computed index values for landslide susceptibility (LSI) in six models, which were then categorized into five subclasses (Very Low, Low, Medium, High and Very High) via the natural breaks (Jenks, 1967) classification method. Subsequently, LSMs were generated for all three study areas (Fig. 6, Fig. 7, Fig. 8). Natural breaks is the most commonly used classification method for the generation of LSMs (Youssef and Pourghasemi, 2021; Padhan et al., 2023; Usta et al., 2024). Guo et al. (2021) stated that natural breaks classification method makes the LSI classification result more objective.

The distribution of susceptibility classes in six models for the study area covering Hopa and Kemalpaşa districts is given in Fig. 9. On average, it was found that the susceptibility to landslides was very low in 7 % of this study area, low in 50.92 %, moderate in 18.60 %, high in 13.65 % and very high in 9.84 %. Upon visual examination of Fig. 9, it is evident that the susceptibility classes are evenly divided throughout all six models. The distribution of areas highly susceptible to landslides in Model_1, Model_2, Model_3, Model_4, Model_5 and Model_6 was as follows, respectively: 14.14 %, 14.15 %, 13.49 %, 13.77 %, 13.08 % and 13.25 %. Similarly, 8.99 % in Model_1, 9.82 % in Model_2,

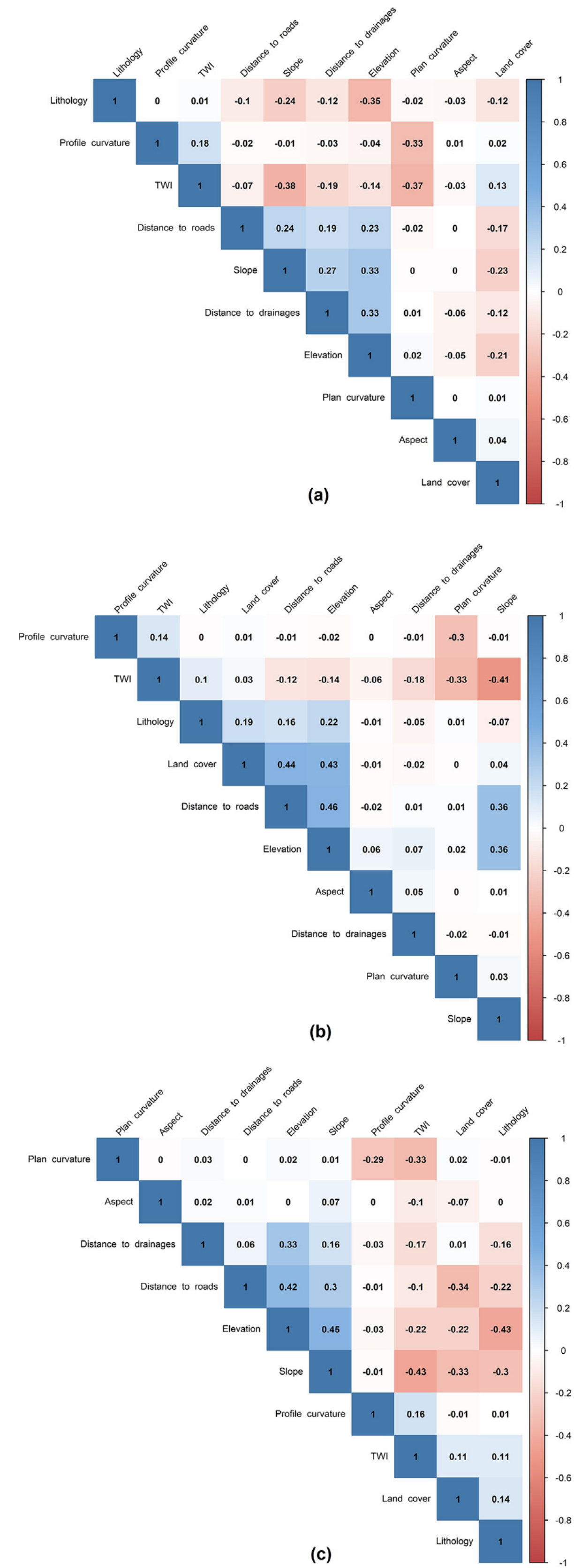

Fig. 5. Correlation matrices for study areas: (a) Hopa, Kemalpaşa, (b) Ardeşen, Fındıklı, (c) Ortahisar, Yomra, Arsin.

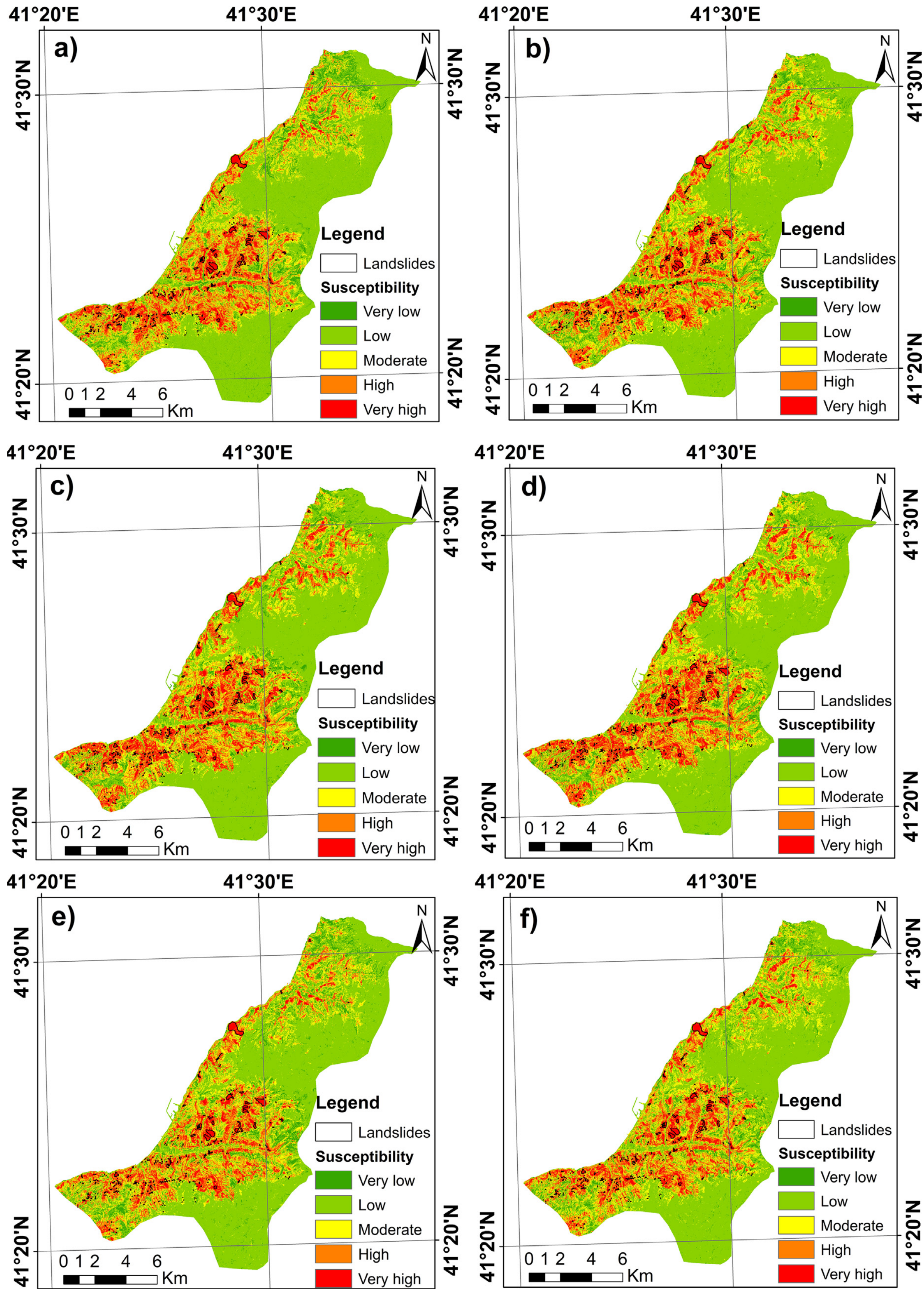

Fig. 6. LSMs for Hopa and Kemalpaşa: a) Model_1, b) Model_2, c) Model_3, d) Model_4, e) Model_5, and f) Model_6.

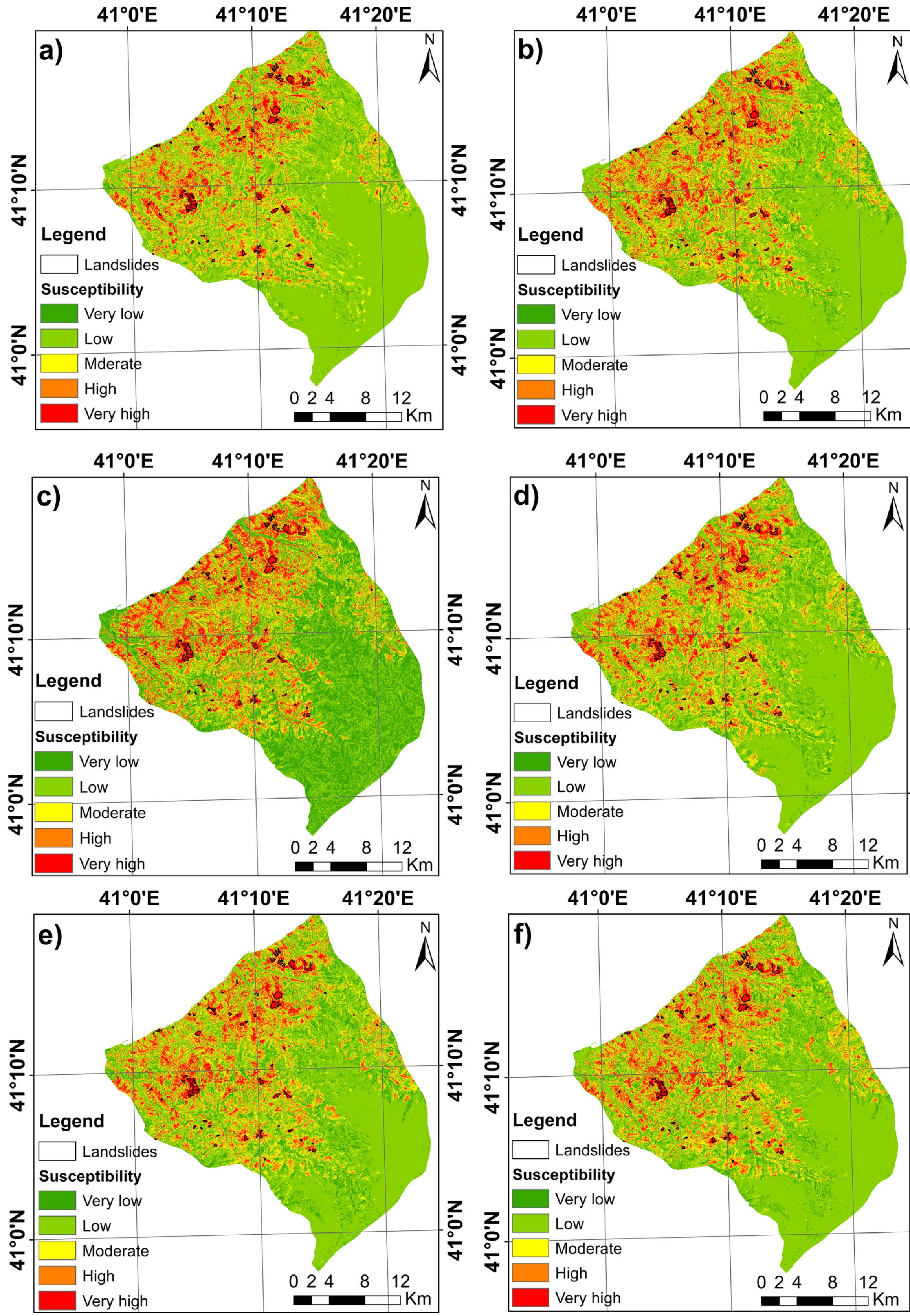

Fig. 7. LSMs for Ardeşen and Fındıklı: (a) Model_1, (b) Model_2, (c) Model_3, (d) Model_4, (e) Model_5, and (f) Model_6.

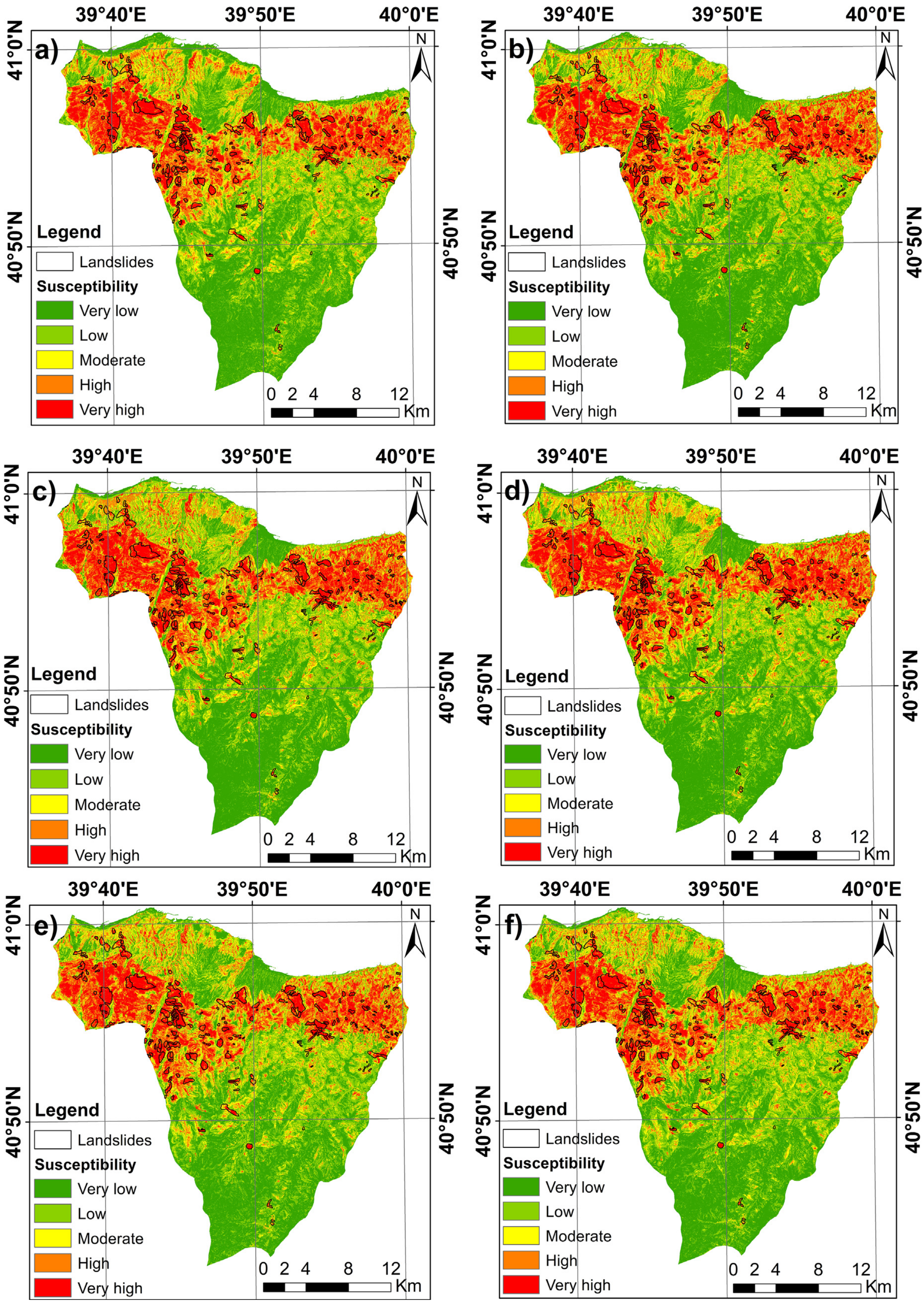

Fig. 8. LSMs for Ortahisar, Yomra and Arsin: (a) Model_1, (b) Model_2, (c) Model_3, (d) Model_4, (e) Model_5, and (f) Model_6.

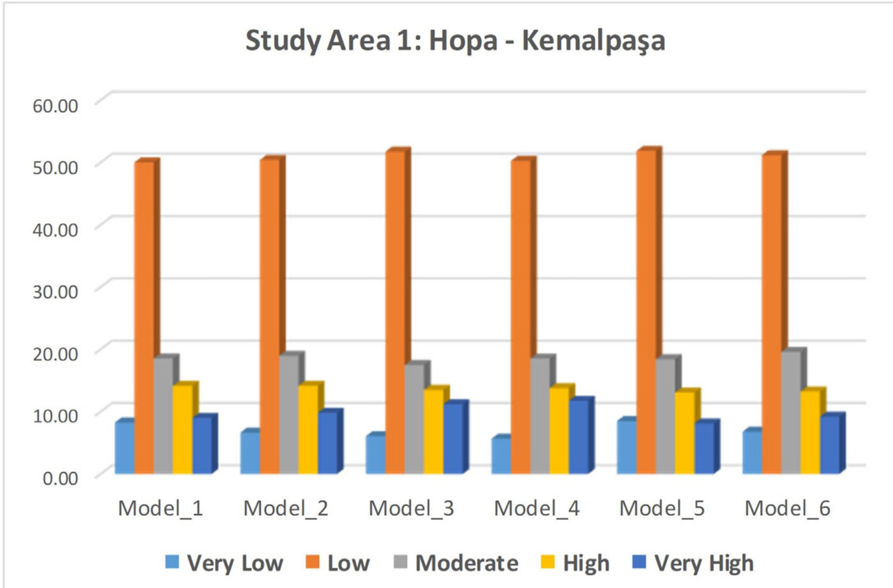

Fig. 9. Percentage distribution of susceptibility classes in Hopa and Kemalpaşa districts in six models.

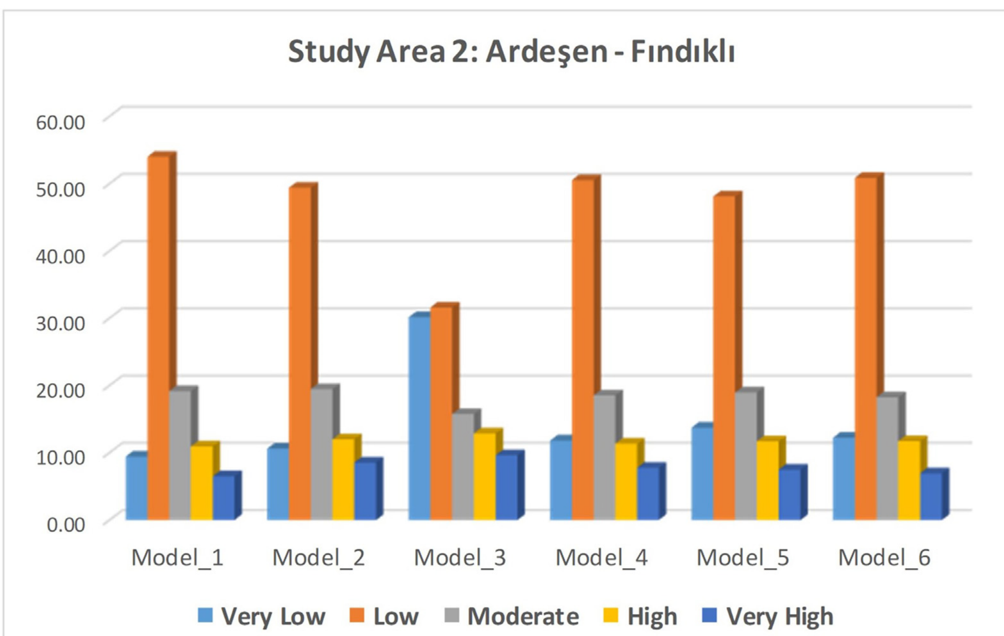

Fig. 10. Percentage distribution of susceptibility classes in Ardeşen and Fındıklı districts in six models.

11.18 % in Model_3, 11.75 % in Model_4, 8.11 % in Model_5 and 9.18 % in Model_6 of the research region were discovered to be extremely prone to landslides.

The distribution of susceptibility classes in six models for the second study area covering Ardeşen and Fındıklı districts is given in Fig. 10. On average, 14.66 %, 47.42 %, 18.36 %, 11.77 %, 11.77 %, and 7.8 % of this study area was found to have very low, low, medium, high, and very high susceptibility to landslides, respectively. When Fig. 10 is examined visually, it is seen that the susceptibility classes show an approximately homogeneous distribution in five models, while the distribution differs in Model_3, where the equal interval classification method is used. The distributions of highly landslide susceptible areas in Model_1, Model_2, Model_3, Model_4, Model_5 and Model_6 were as follows, respectively: 10.95 %, 12 %, 12.88 %, 11.35 %, 11.70 % and 11.72 %. Similarly, 6.48 % of the study area in Model_1, 8.53 % in Model_2,

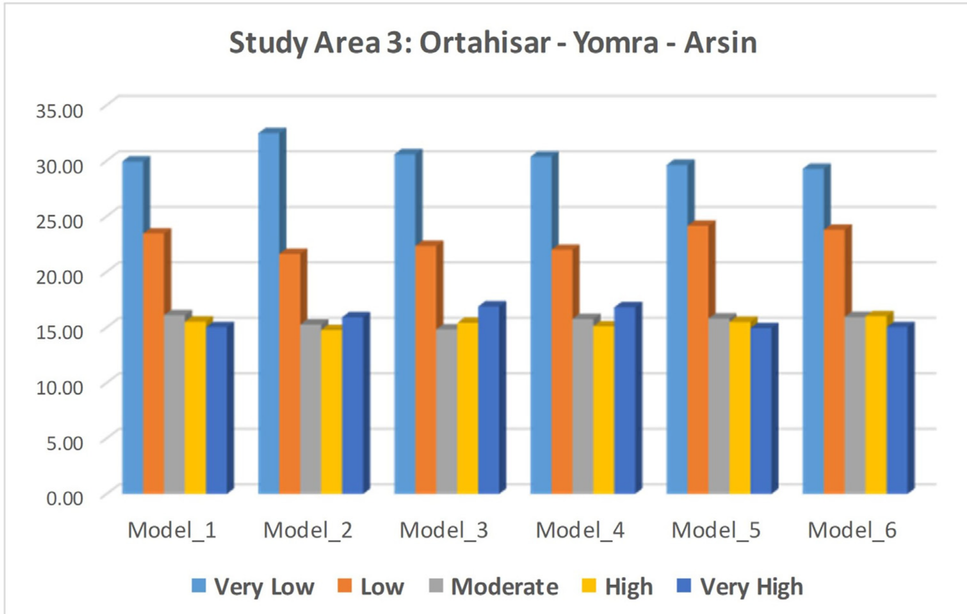

Fig. 11. Percentage distribution of susceptibility classes in Ortahisar, Yomra and Arsin districts in six models.

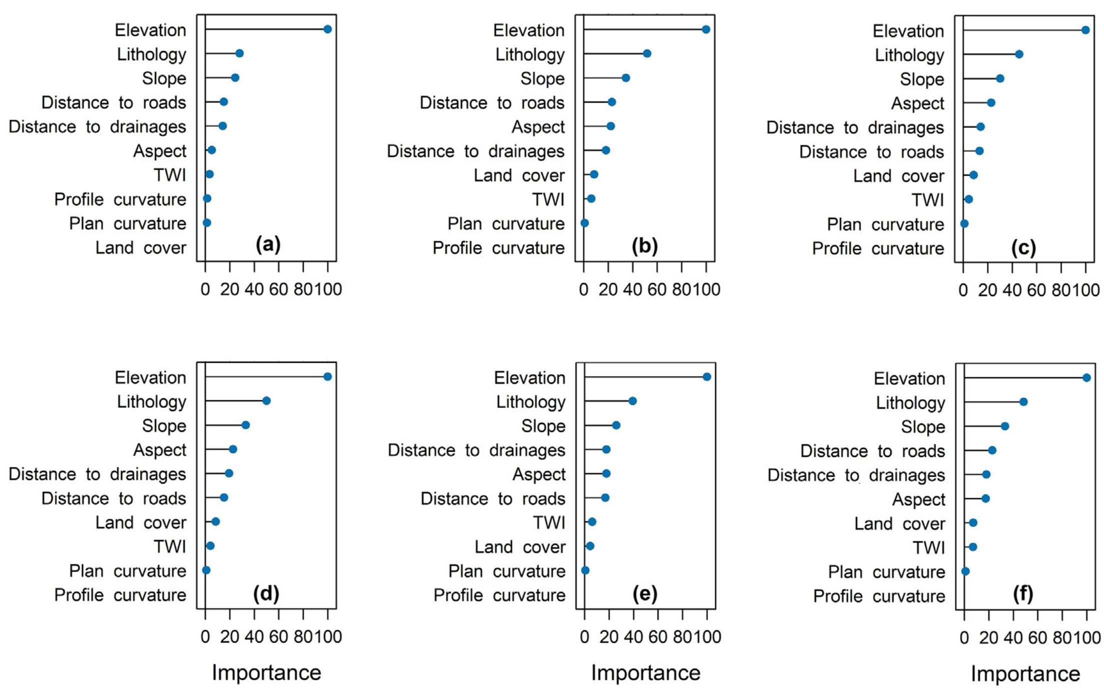

Fig. 12. Importance of conditioning factor for Hopa-Kemalpaşa: (a) continuous, (b) natural breaks, (c) equal interval, (d) manual, (e) quantile, (f) geometric interval.

9.63 % in Model_3, 7.76 % in Model_4, 7.48 % in Model_5 and 6.93 % in Model_6 were found to be very highly susceptible to landslides.

The distribution of susceptibility classes in six models for the third study area covering Ortahisar, Yomra, and Arsin districts of Trabzon is given in Fig. 11. On average, 30.38 %, 22.89 %, 15.60 %, 15.38 % and 15.76 % of this study area was found to have very low, low, medium, high and very high susceptibility to landslides, respectively. When Fig. 11 is examined visually, it is seen that the susceptibility classes show an approximately homogeneous distribution in all six models. The distributions of highly landslide susceptible areas in Model_1, Model_2, Model_3, Model_4, Model_5 and Model_6 were as follows, respectively: 15.51 %, 14.76 %, 15.40 %, 15.10 %, 15.49 % and 15.99 %. Similarly, 15.02 % of the study area in Model_1,

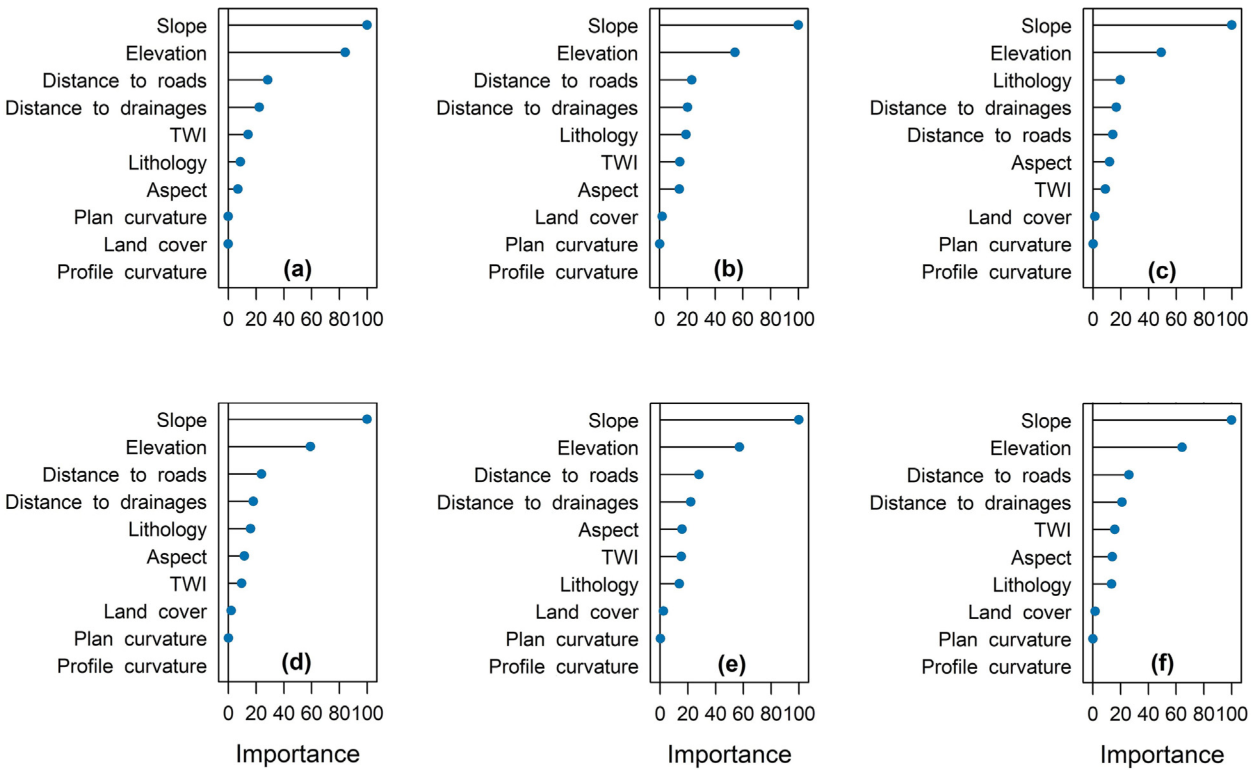

Fig. 13. Importance of conditioning factor for Ardeşen-Fındıklı: (a) continuous, (b) natural breaks, (c) equal interval, (d) manual, (e) quantile, (f) geometric interval.

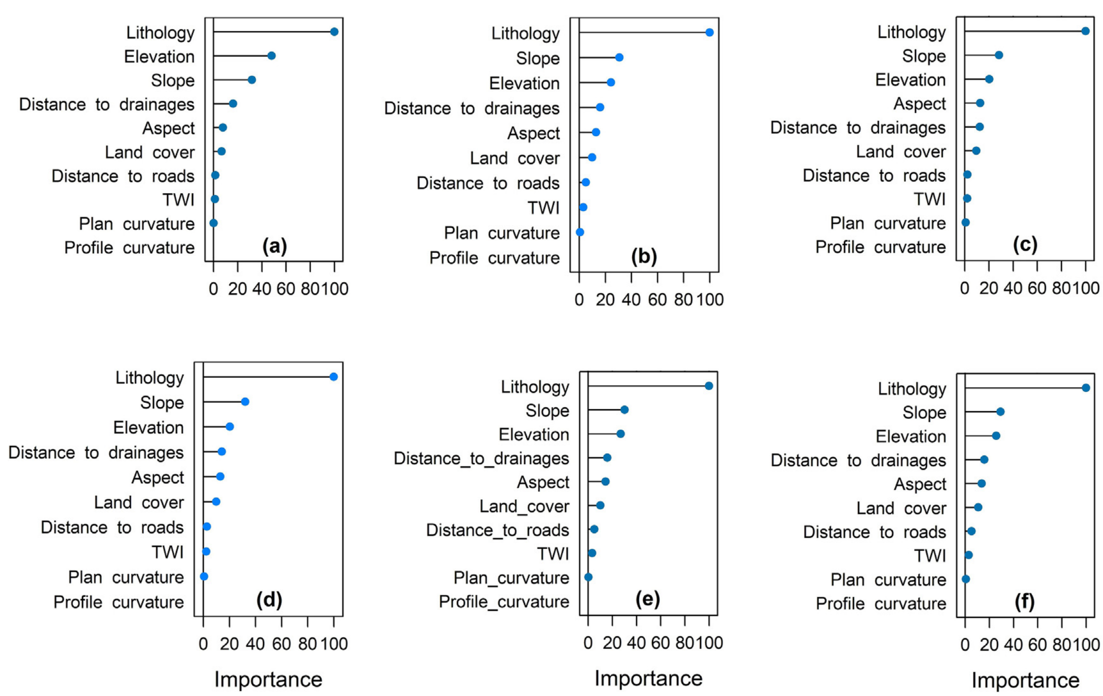

Fig. 14. Importance of conditioning factor for Ortahisar-Yomra-Arsin: (a) continuous, (b) natural breaks, (c) equal interval, (d) manual, (e) quantile, (f) geometric interval.

15.90 % in Model_2, 16.87 % in Model_3, 16.80 % in Model_4, 14.93 % in Model_5 and 15.02 % in Model_6 were found to be very highly susceptible to landslides.

As mentioned in Section 2.1, Trabzon is a city with the highest number of landslides across the Eastern Black Sea Zone. Thus, in the third study region encompassing the dis-

Table 7
AUC values for success rate and prediction rate curves.

ROC Curve	Study Area	Model_1 (Continuos)	Model_2 (Nat. B.)	Model_3 (Equal Int.)	Model_4 (Manual)	Model_5 (Quantile)	Model_6 (Geo. Int.)
Success rate	Hopa/Kemalpaşa	**0.993**	0.974	0.963	0.965	0.984	0.981
	Ardeşen/Fındıklı	**0.991**	0.969	0.955	0.973	0.975	0.979
	Ortahisar/Yomra/Arsin	**0.929**	0.905	0.893	0.899	0.916	0.909
Prediction rate	Hopa/Kemalpaşa	**0.964**	0.952	0.941	0.943	0.961	0.958
	Ardeşen/Fındıklı	**0.986**	0.968	0.955	0.972	0.973	0.975
	Ortahisar/Yomra/Arsin	**0.908**	0.897	0.887	0.892	0.905	0.900

tricts of Trabzon, the proportion of land highly and very highly prone to landslides is greater (averaging 31.13 % of the total area) compared to the other two study areas.

3.3. Analysis of landslide conditioning factors

Effective mitigation against damages incurred by landslides requires an accurate understanding of the factors that control and generate landslides within a given area (Çan and Duman, 2017). For this reason, in LS mapping studies, the importance of conditioning factors should be calculated and the factors that are most or least effective in landslide formation should be identified. Shahzad et al. (2022) emphasized that determining the importance of causal factors is one of the important analyses in machine learning and LSMs. Thus, decision-makers can be informed about which factors should be prioritized to reduce landslide damage in the region where LS mapping study is carried out.

The feature importance graph of six XGBoost-based models for Hopa and Kemalpaşa districts is shown in Fig. 12. In all models, slope, lithology, and elevation were determined to have the greatest effects on the likelihood of landslides. Similar findings were made on the factors that had the least influence on landslides in this study area: land cover, TWI, plan curvature, and profile curvature. The findings align with previous research in the field. The most effective factors, according to Akinci et al. (2020), which covered the districts of Arhavi, Hopa, and Kemalpaşa, were lithology, slope, and elevation; the least successful elements, according to the study, were TWI and curvature. Çan and Duman (2017) analyzed the relationship between landslides triggered by excessive rainfall and environmental factors on August 24, 2015 in Hopa district and found that there was a relationship between landslides and elevation and slope. The researchers found that 80 % of landslides occurred at altitudes below 350 m and 77 % of landslides occurred on hillsides with a slope between 15° and 35°.

The feature importance graph of the models for Ardeşen and Fındıklı districts is shown in Fig. 13. The study found that slope, elevation, distance to roads, and distance to drainages were the primary elements influencing the landslides' occurrence. On the other hand, land cover, plan curvature and profile curvature had the least impact on landslides. The LS study conducted by Yavuz Ozalp et al. (2023) yielded comparable findings in the same research area, employing RF, GBM, CatBoost, and XGBoost algorithms. The scientists found that land cover, plan and profile curvature had the lowest efficacy in influencing the formation of landslides. Similarly, slope and elevation were determined as the most effective factors. Similar results were found in the LS mapping study carried out in the Fındıklı region by Akgun et al. (2008). For example, the researchers have found that hillsides with a slope value of 20–30° and areas closer than 50 m to roads have a high probability of landslides.

The importance levels of factors for Ortahisar, Yomra and Arsin are shown in Fig. 14. The most significant determinants of landslide occurrence in this research area were found to be lithology, slope, elevation, and distance to drainages. As in Hopa and Kemalpaşa districts, the factors of TWI, plan curvature, and profile curvature were determined to have the least impact. Akgün and Bulut (2007) conducted a study on landslide susceptibility in Yomra and Arsin. They included aspect, slope, distance from drainage, distance from roads, and weathered lithological units as conditioning factors. Researchers discovered that weathered lithologic units and slope are the most relevant factors for predicting landslide risk in the study area. Kavzoglu et al. (2014) did a study on landslides in Trabzon and found that lithology and slope are the factors with the highest weights (hence the most important factors).

3.4. Comparison and validation of ML models

Various metrics or methodologies are used to assess the effectiveness of LS models. Some of these metrics are overall accuracy, precision, and the area under the receiver operating characteristic curve (AUC-ROC). However, when we examine the LS mapping literature, we see that the most widely used performance evaluation method is AUC-ROC (Youssef and Pourghasemi, 2021; Padhan et al., 2023; Zhou et al., 2024). A graph known as the ROC curve displays the false positive rate (FPR or 1-

specificity) on the horizontal axis and the true positive rate (TPR or sensitivity) on the vertical axis (Ye et al., 2022). TPR and FPR are defined in Eqs. (1) and (2).

$$TPR = Sensitivity = \frac{TP}{TP + FN} \tag{1}$$

$$FPR = 1 - Specificity = \frac{FP}{TN + FP} \tag{2}$$

The formulas contain components of the confusion matrix, which are TP, TN, FP, and FN. TP is the proportion of samples that, according to the model's prediction result, are landslides and are classified as such. TN is the number of samples that, according to the prediction, were classified as non-landslides even though they were not landslides in the first place. False Positive (FP) refers to the count of samples that were incorrectly classified as landslides when they were actually non-landslides, based on the prediction. FN represents the count of samples that were truly landslides but were misclassified as non-landslides due to the prediction (Tang et al., 2023; Alkan Akinci et al., 2024). The accuracy or performance of a susceptibility model is usually measured by the AUC value. This value, which falls between 0.5 and 1.0, is generally categorized into five grades: poor (0.5–0.6), fair (0.6–0.7), good (0.7–0.8), very good (0.8–0.9) and excellent (0.9–1.0) (Wei et al., 2022; Ye et al., 2022; Yavuz Ozalp et al., 2023).

In LSM studies, performance evaluations are generally made with two different ROC curves. These are success rate and prediction rate curves (Vakhshoori et al., 2019; Chen et al., 2020; Chowdhury et al., 2024). The success rate curve generated from the training dataset depicts the model's ability to accurately classify the known landslide sites in the training dataset, or its ability to accurately represent the data. The test data set is used to generate the prediction rate curve, which describes how effectively the model predicts unknown or future landslides (Wubalem, 2021; Yavuz Ozalp et al., 2023; Chowdhury et al., 2024).

Table 7 shows the AUC values of the success and prediction rate curves generated for the six models utilized in this investigation. In all three study areas, Model_1 had the highest AUC in both the training and validation stages. In Model_1, elevation, slope, plan and profile curvature, TWI, distance to drainage networks and distance to road were used as continuous data without reclassification. In all three study areas, the lowest AUC values were obtained from Model_3, where factors were reclassified with equal intervals (Table 7). The validation results obtained according to the prediction rate indicate that the susceptibility model's accuracy improves when the spatial data of conditioning factors other than discrete factors are used as continuous data.

4. Discussion

LS mapping studies around the world have largely focused on the development of high-performance susceptibility models that enable the production of accurate and reliable LSMs. For this purpose, either a large number of models have been compared (Pourghasemi and Rahmati, 2018; Lu et al., 2023; Usta et al., 2024), novel methodologies have been tried (Gu et al., 2024; Xu et al., 2024; Yu and Chen, 2024), or hybrid (combining) models have been developed (Kıncal and Kayhan, 2022; Wang et al., 2024; Zhou et al., 2024). Despite this worldwide effort, we see that the optimal model or approach for LSM production is not clear, nor has a widely accepted methodology been developed (Ye et al., 2022; Wei et al., 2022). This shows that the search will continue in the coming years.

The research area's susceptibility to landslides is indicated by the LSI values produced using the LS model for each pixel. There is a direct correlation between the LSI value of a pixel and the likelihood of a landslide occurring within the pixel. According to Wubalem (2021), a lower LSI indicates a decreased likelihood of landslides. LSMs are created by reclassifying these LSI values calculated by susceptibility models. Researchers use different classification methods in this classification process. Although there is a widely accepted number of classes (very low, low, moderate, high, and very high), it is evident that there are doubts over the most preferable approach for classifying LSIs. Although natural breaks (Yao et al., 2023; Ye et al., 2023; Chowdhury et al., 2024) is commonly used to classify LSIs, various studies with different classification methods including equal interval (Sun et al., 2023b; Tang et al., 2023; Zhang et al., 2023), standard deviation (Dağ et al., 2020), or quantile (Zhao and Chen, 2020; Thi Ngo et al., 2021; Sahin, 2022).

On the other hand, a large number of conditioning factors are taken into account in the production of LSMs. Some factors such as elevation, slope and TWI are continuous, while others (such as aspect, lithology and land cover) are discrete or categorical. Factors in continuous structure are transformed into discrete structure using various classification methods and then introduced as input to the models (Sahin, 2020). At this stage, we see that researchers prefer different classification methods and different class numbers. For example, Sahin (2020) reclassified all continuous factors into eight subclasses with natural breaks classification method in his LS mapping study using GBM, RF and XGBoost algorithms in Sinop, a province located in Turkey's Black Sea region. Kilicoglu (2021), on the other hand, reclassified some factors (elevation, slope, distance to fault lines, distance to drainage network) into 10 subclasses with equal intervals, while some factors (e.g. TWI) were separated into five subclasses with the natural breaks classification technique. Zhao and Chen (2023) stated that the preprocessing of discretization of conditioning factors has not been fully investigated or taken into account in studies. The researchers emphasized that the selection of the number of intervals for discretization methods and landslide-related conditioning factors is subjective and random, and this will have an effect on how well the LSM works. Hence, the objective of this study was to examine the impact for various data classification techniques on the ultimate accuracy of LSMs. However, the issue of what the optimum number of classes should be was not addressed in this study and is left for future studies.

The results of our experimental study are given in Table 7. In all three study areas, it was determined that Model_1, which uses a combination of discrete and continuous factors in both training and validation stages, had the highest AUC values compared to the others. Based on the AUC values of the prediction rate curves, it was found that not using discretization methods caused an average improvement of 1.3 % in the first study area, 1.74 % in the second study area and 1.18 % in the third study area. This shows that when a continuous factor is transformed into a categorical factor, there is a slight loss of information, which impacts the correlation between the factor and the occurrence of landslides. Indeed, Pasta (2009) emphasized that if a variable has a strictly linear relationship with the outcome, turning a continuous variable into a categorical one causes some degree of information loss.

On the other hand, when the histograms of elevation, slope and TWI datasets in all three study areas are examined, it is seen that they are skewed to the right. The histograms of distance to road and distance to drainages show a heavy-tailed distribution. In a heavy-tailed distribution, an example of a right skewed distribution, there are large values at the head of the histogram that cover a low percentage (minority), while small values are concentrated in the long tail and cover a high percentage or majority (Jiang, 2013). It is known that when the data are not normally distributed or skewed, equal interval classes do not represent the data distribution well (many data in one class and few data in others) and lead to biased classification results (Li and Shan, 2022). For this reason, Model_3 was found to perform relatively lower than the other models. Since the Models 2, 5 and 6 have AUC values of 0.9 and above in all the study areas, it would be more accurate to evaluate these models within their respective contexts. Model_5 using the quantile classification method, Model_6 using the geometric interval method and Model_2 using the natural breaks classification method were the best performing models after Model_1. The quantile classification method, which helps to reduce the effect of outliers, and the geometric interval classification method give good results especially in the classification and visualization of continuous data where the data distribution is skewed (Li and Shan, 2022; Campbell et al., 2023). Therefore, Model_5 and Model_6 are the best performing models after Model_1. When Table 7 is examined, it is seen that Model_2, which uses the natural breaks classification method, lags behind Model_5 and Model_6. This is because the natural breaks classification method works best with unevenly distributed and not skewed data.

Ultimately, while this research enhances the precision of LSM predicted using machine learning techniques, it does possess certain constraints. The first one is related to the number of ML algorithms used. In this study, only one ML algorithm (XGBoost) was used. As with the number of study areas, the number of algorithms can be increased to evaluate whether similar results are obtained with different algorithms. The second limitation is related to determining the optimum number of classes in the discretization phase. At this stage, it was considered that the methodology used by Zhao and Chen (2023) could be used.

5. Conclusions

This study examined how distinct discretization methods affected the precision of LSMs. In the study, considering the results of the multicollinearity analysis, LSMs of three different study areas were produced with ten conditioning factors that are commonly used in the literature. XGBoost algorithm is used in the ML-based susceptibility model. The study areas were selected from three different provinces in the Eastern Black Sea Region, one of Turkey's most landslide-prone regions. Six XGBoost-based models were developed for each study area. Aspect, lithology and land cover were provided as discrete data to all models. In the first model, no discretization method was used, and discrete and continuous factors were introduced as input to the model together. Continuous factors were divided into nine subclasses using natural breaks in the second model, equal interval in the third model, manual in the fourth model, quantile in the fifth model, and geometric interval in the sixth model. The optimum number of classes was not investigated in this study and the factors (other than plan curvature and profile curvature) were divided into nine subclasses to be line with aspect. The empirical findings in three different study areas demonstrate that the model using a combination of discrete and continuous factors outperforms the other models using discretization methods. The model without the discretization method outperformed the other models by 2.2 % on average in the training phase and 1.4 % on average in the validation phase. It is a well-known fact that worldwide efforts to produce reliable and accurate LSMs will continue in the coming years. This work aims to enhance the existing literature on the selection of discretization methods for the creation of LSMs. In addition, the methodology utilized in this study has the potential to be employed in many susceptibility mapping studies, not limited to LSM, by including diverse machine learning models.

Declaration of competing interest

The authors declare that they have no known competing financial interests or personal relationships that could have appeared to influence the work reported in this paper.

Appendix A. Supplementary material

Supplementary material to this article can be found online at https://doi.org/10.1016/j.asr.2024.12.020.

References

Abraham, M.T., Satyam, N., Lokesh, R., Pradhan, B., Alamri, A., 2021. Factors affecting landslide susceptibility mapping: assessing the influence of different machine learning approaches, sampling strategies and data splitting. Land 10, 989. https://doi.org/10.3390/land10090989.

Aditian, A., Kubota, T., Shinohara, Y., 2018. Comparison of GIS-based landslide susceptibility models using frequency ratio, logistic regression, and artificial neural network in a tertiary region of Ambon, Indonesia. Geomorphology 318, 101–111. https://doi.org/10.1016/j.geomorph.2018.06.006.

Ajim Ali, S., Parvin, F., Pham, Q.B., Khedher, K.M., Dehbozorgi, M., Rabby, Y.W., Anh, D.T., Nguyen, D.H., 2022. An ensemble random forest tree with SVM, ANN, NBT, and LMT for landslide susceptibility mapping in the Rangit River watershed, India. Nat. Hazards 113, 1601–1633. https://doi.org/10.1007/s11069-022-05360-5.

Akgün, A., Bulut, F., 2007. GIS-based landslide susceptibility for Arsin-Yomra (Trabzon, North Turkey) region. Environ. Geol. 51, 1377–1387. https://doi.org/10.1007/s00254-006-0435-6.

Akgun, A., Dag, S., Bulut, F., 2008. Landslide susceptibility mapping for a landslide-prone area (Findikli, NE of Turkey) by likelihood-frequency ratio and weighted linear combination models. Environ. Geol. 54, 1127–1143. https://doi.org/10.1007/s00254-007-0882-8.

Akinci, H., 2022. Assessment of rainfall-induced landslide susceptibility in Artvin, Turkey using machine learning techniques. J. Afr. Earth Sci. 191, 104535. https://doi.org/10.1016/j.jafrearsci.2022.104535.

Akinci, H., Kilicoglu, C., Dogan, S., 2020. Random forest-based landslide susceptibility mapping in coastal regions of Artvin, Turkey. ISPRS Int. J. Geo-Inf. 9, 553. https://doi.org/10.3390/ijgi9090553.

Akinci, H., Yavuz Ozalp, A., 2021. Landslide susceptibility mapping and hazard assessment in Artvin (Turkey) using frequency ratio and modified information value model. Acta Geophys. 69, 725–745. https://doi.org/10.1007/s11600-021-00577-7.

Alkan Akıncı, H., Akıncı, H., 2023. Machine learning based forest fire susceptibility assessment of Manavgat district (Antalya), Turkey. Earth Sci. Inf. 16, 397–414. https://doi.org/10.1007/s12145-023-00953-5.

Alkan Akinci, H., Akinci, H., Zeybek, M., 2024. Comparison of diverse machine learning algorithms for forest fire susceptibility mapping in Antalya, Türkiye. Adv. Space Res. 74, 647–667. https://doi.org/10.1016/j.asr.2024.04.018.

Aslam, B., Zafar, A., Khalil, U., 2023. Comparative analysis of multiple conventional neural networks for landslide susceptibility mapping. Nat. Hazards 115, 673–707. https://doi.org/10.1007/s11069-022-05570-x.

Baeza, C., Lantada, N., Amorim, S., 2016. Statistical and spatial analysis of landslide susceptibility maps with different classification systems. Environ. Earth Sci. 75, 1318. https://doi.org/10.1007/s12665-016-6124-1.

Bammou, Y., Benzougagh, B., Abdessalam, O., Brahim, I., Kader, S., Spalevic, V., Sestras, P., Ercişli, S., 2024. Machine learning models for gully erosion susceptibility assessment in the Tensift catchment, Haouz Plain, Morocco for sustainable development. J. Afr. Earth Sci. 213, 105229. https://doi.org/10.1016/j.jafrearsci.2024.105229.

Barman, J., Das, J., 2024. Assessing classification system for landslide susceptibility using frequency ratio, analytical hierarchical process and geospatial technology mapping in Aizawl district, NE India. Adv. Space Res. 74 (3), 1197–1224. https://doi.org/10.1016/j.asr.2024.05.007.

Brabb, E.E., 1993. Proposal for worldwide landslide hazard maps. In: Proceedings of the Seventh International Conference and Field Workshop on Landslides in Czech and Slovak Republics, Czech Republic and Slovakia, 28 August–15 September 1993. Rotterdam, Brookfield, VT, USA, pp. 15–27.

Campbell, J.E., Shin, M., 2012. Geographic information system basics. v. 1.0. https://2012books.lardbucket.org/pdfs/geographic-information-system-basics.pdf. Accessed 1 Nov 2016.

Campbell, J.E., Sedani, A.E., Dao, H.D.N., Sambo, A., Doescher, M., Janitz, A., 2023. Investigation of geographical disparities: The use of an interpolation method for cancer registry data. J. Okla. State Med. Assoc. 116 (2), 62–71.

Çan, T., Duman, T., 2017. Rainfall intensity - duration relationship and event landslide inventory of Hopa (Eastern Black Sea) Region. MÜHJEO'2017 National Symposium on Engineering Geology and Geotechnics.

Can, R., Kocaman, S., Gokceoglu, C., 2021. A comprehensive assessment of XGBoost algorithm for landslide susceptibility mapping in the upper basin of Ataturk Dam, Turkey. Appl. Sci. 11, 4993. https://doi.org/10.3390/app11114993.

Cao, J., Zhang, Z., Du, J., Zhang, L., Song, Y., Sun, G., 2020. Multi geohazards susceptibility mapping based on machine learning—a case study in Jiuzhaigou, China. Nat. Hazards 102, 851–871. https://doi.org/10.1007/s11069-020-03927-8.

Chang, L., Xing, G., Yin, H., Fan, L., Zhang, R., Zhao, N., Huang, F., Ma, J., 2023. Landslide susceptibility evaluation and interpretability analysis of typical loess areas based on deep learning. Nat. Hazards Res. 3, 155–169. https://doi.org/10.1016/j.nhres.2023.02.005.

Chen, X., Chen, W., 2021. GIS-based landslide susceptibility assessment using optimized hybrid machine learning methods. Catena 196, 104833. https://doi.org/10.1016/j.catena.2020.104833.

Chen, T., Guestrin, C., 2016. Xgboost: A scalable tree boosting system. In: Proceedings of the 22nd ACM SIGKDD International Conference on Knowledge Discovery and Data Mining, August 2016, pp. 785–794. https://doi.org/10.1145/2939672.2939785.

Chen, W., Xie, X., Peng, J., Shahabi, H., Hong, H., Tien Bui, D., Duan, Z., Li, S., Zhu, A.X., 2018. GIS-based landslide susceptibility evaluation using a novel hybrid integration approach of bivariate statistical based random forest method. Catena 164, 135–149. https://doi.org/10.1016/j.catena.2018.01.012.

Chen, T., Zhu, L., Niu, R.-Q., Trinder, C.J., Peng, L., Lei, T., 2020. Mapping landslide susceptibility at the Three Gorges Reservoir, China, using gradient boosting decision tree, random forest, and information value models. J. Mt. Sci. 17, 670–685. https://doi.org/10.1007/s11629-019-5839-3.

Chowdhury, Md.S., Rahman, Md.N., Sheikh, Md.S., Sayeid, Md.A., Mahmud, K.H., Hafsa, B., 2024. GIS-based landslide susceptibility mapping using logistic regression, random forest and decision and regression tree models in Chattogram District, Bangladesh. Heliyon 10, e23424. https://doi.org/10.1016/j.heliyon.2023.e23424.

ClimateData, 2024. Climate Hopa (Turkey). https://www.deepl.com/translator#tr/en/%C4% B0klim%20Hopa%20(T%C3%BCrkiye). Accessed 9 May 2024.

CLMS, 2020. CORINE Land Cover 2018 (vector/raster 100 m), Europe, 6-yearly. European Union's Copernicus Land Monitoring Service Information. https://doi.org/10.2909/71c95a07-e296-44fc-b22b-415f42acfdf0.

Dağ, S., Akgün, A., Kaya, A., Alemdağ, S., Bostancı, H.T., 2020. Medium scale earthflow susceptibility modelling by remote sensing and geographical information systems based multivariate statistics approach: an example from Northeastern Turkey. Environ. Earth Sci. 79, 468. https://doi.org/10.1007/s12665-020-09217-7.

Daoud, J.I., 2017. Multicollinearity and regression analysis. J. Phys. Conf. Ser. 949. https://doi.org/10.1088/1742-6596/949/1/012009 012009.

Dawson, G., Butt, J., Jones, A., Fraccaro, P., 2023. Flood susceptibility mapping at the country scale using machine learning approaches. Appl. Ai Lett. 4 (4), e88.

de Smith, M.J., Goodchild, M.F., Longley, P.A., 2018. Geospatial Analysis: A Comprehensive Guide to Principles, 6th ed. The Winchelsea Press, London.

Demirağ Turan, İ., Özkan, B., Türkeş, M., Dengiz, O., 2020. Landslide susceptibility mapping for the Black Sea Region with spatial fuzzy multi-criteria decision analysis under semi-humid and humid terrestrial ecosystems. Theor. Appl. Climatol. 140, 1233–1246. https://doi.org/10.1007/s00704-020-03126-2.

DEMP, 2018. Disaster management and natural disaster statistics in Turkey. https://www.afad.gov.tr/kurumlar/afad.gov.tr/35429/xfiles/-turkiye_de_afetler.pdf. Accessed 19 Jan 2023.

Dilley, M., Chen, R.S., Deichmann, U., Lerner-Lam, A.L., Arnold, M., Agwe, J., Buys, P., Kjekstad, O., Lyon, B., Yetman, G., 2005. Natural Disaster Hotspots: A Global Risk Analysis. World Bank, Washington, DC.

Dou, H., He, J., Huang, S., Jian, W., Guo, C., 2023. Influences of non-landslide sample selection strategies on landslide susceptibility mapping by machine learning. Geomat. Nat. Haz. Risk 14 (1). https://doi.org/10.1080/19475705.2023.2285719 2285719.

Duman, T.Y., Çan, T., 2023. Characteristics of landslides and assessment of deep-seated landslide susceptibility in Northern Turkey. Mediterr. Geosci. Rev. 5, 131–157. https://doi.org/10.1007/s42990-023-00105-3.

ESRI, 2024a. Data classification methods. https://pro.arcgis.com/en/pro-app/latest/help/mapping/layer-properties/data-classification-methods.htm. Accessed 14 May 2024.

ESRI, 2024b. How XGBoost algorithm works. https://pro.arcgis.com/en/pro-app/latest/tool-reference/geoai/how-xgboost-works.htm. Accessed 19 November 2024.

Gariano, S.L., Guzzetti, F., 2016. Landslides in a changing climate. Earth Sci. Rev. 162, 227–252. https://doi.org/10.1016/j.earscirev.2016.08.011.

GDM, 2024a. Climate classification Artvin – Hopa, General Directorate of Meteorology. https://www.mgm.gov.tr/iklim/iklim-siniflandirmalari.aspx?m=HOPA. Accessed 7 May 2024.

GDM, 2024b. Official statistics - Rize, General Directorate of Meteorology. https://www.mgm.gov.tr/veridegerlendirme/il-ve-ilceler-istatistik.aspx?k=A&m=RIZE. Accessed 8 May 2024.

GDM, 2024c. Climate classification Rize, General Directorate of Meteorology. https://www.mgm.gov.tr/iklim/iklim-siniflandirmalari.aspx?m=RIZE. Accessed 8 May 2024.

GDM, 2024d. Official statistics – Trabzon, General Directorate of Meteorology. https://www.mgm.gov.tr/veridegerlendirme/il-ve-ilceler-istatistik.aspx?k=A&m=TRABZON. Accessed 9 May 2024.

GDM, 2024e. Climate classification Trabzon, General Directorate of Meteorology. https://www.mgm.gov.tr/iklim/iklim-siniflandirmalari.aspx?m=TRABZON. Accessed 9 May 2024.

Ghorbanzadeh, O., Shahabi, H., Crivellari, A., Homayouni, S., Blaschke, T., Ghamisi, P., 2022. Landslide detection using deep learning and object-based image analysis. Landslides 19, 929–939. https://doi.org/10.1007/s10346-021-01843-x.

Ghorbanzadeh, O., Gholamnia, K., Ghamisi, P., 2023. The application of ResU-net and OBIA for landslide detection from multi-temporal Sentinel-2 images. Big Earth Data 7 (4), 961–985. https://doi.org/10.1080/20964471.2022.2031544.

Ghorbanzadeh, O., Shahabi, H., Piralilou, S.T., Crivellari, A., Cue la Rosa, L.E., Atzberger, C., Li, J., Ghamisi, P., 2024. Contrastive self-supervised learning for globally distributed landslide detection. IEEE Access 12, 118453–118466. https://doi.org/10.1109/ACCESS.2024.3449447.

Gu, T., Duan, P., Wang, M., Li, J., Zhang, Y., 2024. Effects of non-landslide sampling strategies on machine learning models in landslide susceptibility mapping. Sci. Rep. 14, 7201. https://doi.org/10.1038/s41598-024-57964-5.

Guo, X., Fu, B., Du, J., Shi, P., Chen, Q., Zhang, W., 2021. Applicability of susceptibility model for rock and loess earthquake landslides in the eastern Tibetan Plateau. Remote Sens 13, 2546. https://doi.org/10.3390/rs13132546.

Güven, İ.H., 1998. 1:100,000 scale Geological Maps of Türkiye, No: 58, Trabzon-C29 and D29 Map Sheets. General Directorate of Mineral Research and Exploration.

Hong, H., Pourghasemi, H.R., Pourtaghi, Z.S., 2016. Landslide susceptibility assessment in Lianhua County (China): A comparison between a random forest data mining technique and bivariate and multivariate statistical models. Geomorphology 259, 105–118. https://doi.org/10.1016/j.geomorph.2016.02.012.

Hong, H., Tsangaratos, P., Ilia, I., Loupasakis, C., Wang, Y., 2020. Introducing a novel multi-layer perceptron network based on stochastic gradient descent optimized by a meta-heuristic algorithm for landslide susceptibility mapping. Sci. Total Environ. 742, 140549. https://doi.org/10.1016/j.scitotenv.2020.140549.

Huang, S., Chen, L., 2024. Landslide susceptibility mapping using an integration of different statistical models for the 2015 Nepal earthquake in Tibet. Geomat. Nat. Haz. Risk 15 (1), 2396908. https://doi.org/10.1080/19475705.2024.2396908.

Jenks, G.F., 1967. The data model concept in statistical mapping. Int. Yearbook Cartogr. 7, 186–190.

Jennifer, J.J., 2022. Feature elimination and comparison of machine learning algorithms in landslide susceptibility mapping. Environ. Earth Sci. 81, 489. https://doi.org/10.1007/s12665-022-10620-5.

Jiang, B., 2013. Head/tail breaks: A new classification scheme for data with a heavy-tailed distribution. Prof. Geogr. 65, 482–494.

Kalantar, B., Ueda, N., Saeidi, V., Ahmadi, K., Halin, A.A., Shabani, F., 2020. Landslide susceptibility mapping: Machine and ensemble learning based on remote sensing big data. Remote Sens. 12, 1737. https://doi.org/10.3390/rs12111737.

Kavzoglu, T., Sahin, E.K., Colkesen, I., 2014. Landslide susceptibility mapping using GIS-based multi-criteria decision analysis, support vector machines, and logistic regression. Landslides 11, 425–439. https://doi.org/10.1007/s10346-013-0391-7.

Kavzoglu, T., Teke, A., 2022. Predictive performances of ensemble machine learning algorithms in landslide susceptibility mapping using random forest, extreme gradient boosting (XGBoost) and natural gradient boosting (NGBoost). Arab. J. Sci. Eng. 47, 7367–7385. https://doi.org/10.1007/s13369-022-06560-8.

Keskin, İ., 2013. 1:100,000 scale Geological Maps of Türkiye, No: 178, Artvin-F46 Map Sheet. General Directorate of Mineral Research and Exploration, Ankara, Türkiye.

Kilicoglu, C., 2021. Investigation of the effects of approaches used in the production of training and validation data sets on the accuracy of landslide susceptibility mapping models: Samsun (Turkey) example. Arab. J. Geosci. 14, 2106. https://doi.org/10.1007/s12517-021-08312-8.

Kim, J.H., 2019. Multicollinearity and misleading statistical results. Korean J. Anesthesiol. 72 (6), 558–569. https://doi.org/10.4097/kja.19087.

Kıncal, C., Kayhan, H., 2022. A combined method for preparation of landslide susceptibility map in Izmir (Türkiye). Appl. Sci. 12, 9029. https://doi.org/10.3390/app12189029.

Kuhn, M., 2008. Building predictive models in R using the caret package. J. Stat. Software 28 (5), 1–26. https://doi.org/10.18637/jss.v028.i05.

Kurt, A., Buldu, B., Cedimoğlu, İ.H., 2020. Comparing of performances of xgboost and random forest algorithms aimed at network based intrusion detection. International Marmara Sciences Congress (Spring).

Li, S., Shan, J., 2022. Adaptive geometric interval classifier. ISPRS Int. J. Geo Inf. 11, 430. https://doi.org/10.3390/ijgi11080430.

Liu, S., Wang, L., Zhang, W., He, Y., Pijush, S., 2023. A comprehensive review of machine learning-based methods in landslide susceptibility mapping. Geol. J. 58, 2283–2301. https://doi.org/10.1002/gj.4666.

Liu, L.L., Zhang, J., Li, J., Huang, F., Wang, L., 2022. A bibliometric analysis of the landslide susceptibility research (1999–2021). Geocarto Int. 37 (26), 14309–14334. https://doi.org/10.1080/10106049.2022.2087753.

Longley, P.A., Goodchild, M.F., Maguire, D.J., Rhind, D.W., 2005. Geographical Information Systems and Science, 2nd ed. John Wiley & Sons Ltd, England.

Lu, J., Ren, C., Yue, W., Zhou, Y., Xue, X., Liu, Y., Ding, C., 2023. Investigation of landslide susceptibility decision mechanisms in different ensemble-based machine learning models with various types of factor data. Sustainability 15, 13563. https://doi.org/10.3390/su151813563.

Mutlu, B., Nefeslioglu, H.A., Sezer, E.A., Akcayol, M.A., Gokceoglu, C., 2019. An experimental research on the use of recurrent neural networks in landslide susceptibility mapping. ISPRS Int. J. Geo Inf. 8, 578. https://doi.org/10.3390/ijgi8120578.

Nohani, E., Moharrami, M., Sharafi, S., Khosravi, K., Pradhan, B., Pham, B.T., Lee, S., Melesse, A.M., 2019. Landslide susceptibility

mapping using different GIS-based bivariate models. Water 11, 1402. https://doi.org/10.3390/w11071402.
Nurwatik, N., Ummah, M.H., Cahyono, A.B., Darminto, M.R., Hong, J. H., 2022. A comparison study of landslide susceptibility spatial modeling using machine learning. ISPRS Int. J. Geo Inf. 11, 602. https://doi.org/10.3390/ijgi11120602.
Padhan, B., Dikshit, A., Lee, S., Kim, H., 2023. An explainable AI (XAI) model for landslide susceptibility modeling. Appl. Soft Comput. 142, 110324. https://doi.org/10.1016/j.asoc.2023.110324.
Pasta, D.J., 2009. Learning when to be discrete: Continuous vs. categorical predictors. SAS Global Forum.
Pourghasemi, H.R., Gayen, A., Park, S., Lee, C.W., Lee, S., 2018. Assessment of landslide-prone areas and their zonation using logistic regression, LogitBoost, and Naïve Bayes machine-learning algorithms. Sustainability 10, 3697. https://doi.org/10.3390/su10103697.
Pourghasemi, H.R., Rahmati, O., 2018. Prediction of the landslide susceptibility: Which algorithm, which precision. Catena 162, 177–192. https://doi.org/10.1016/j.catena.2017.11.022.
Pourghasemi, H.R., Kornejady, A., Kerlec, N., Shabani, F., 2020. Investigating the effects of different landslide positioning techniques, landslide partitioning approaches, and presence-absence balances on landslide susceptibility mapping. Catena 187, 104364. https://doi.org/10.1016/j.catena.2019.104364.
Pradhan, A.M.S., Kim, Y.T., 2020. Rainfall-induced shallow landslide susceptibility mapping at two adjacent catchments using advanced machine learning algorithms. ISPRS Int. J. Geo Inf. 9, 569. https://doi.org/10.3390/ijgi9100569.
Putriani, E., Wu, Y.M., Chen, C.W., Ismulhadi, A., Fadli, D.I., 2023. Development of landslide susceptibility mapping with a multi-variance statistical method approach in Kepahiang Indonesia. Terr. Atmos. Ocean. Sci. 34, 18. https://doi.org/10.1007/s44195-023-00050-6.
Saha, S., Roy, J., Pradhan, B., Hembram, T.K., 2021. Hybrid ensemble machine learning approaches for landslide susceptibility mapping using different sampling ratios at East Sikkim Himalayan, India. Adv. Space Res. 68 (7), 2819–2840. https://doi.org/10.1016/j.asr.2021.05.018.
Sahin, E.K., 2020. Assessing the predictive capability of ensemble tree methods for landslide susceptibility mapping using XGBoost, gradient boosting machine, and random forest. SN Appl. Sci. 2, 1308. https://doi.org/10.1007/s42452-020-3060-1.
Sahin, E.K., 2022. Comparative analysis of gradient boosting algorithms for landslide susceptibility mapping. Geocarto Int. 37 (9), 2441–2465. https://doi.org/10.1080/10106049.2020.1831623.
Sahin, E.K., Colkesen, I., 2021. Performance analysis of advanced decision tree-based ensemble learning algorithms for landslide susceptibility mapping. Geocarto Int. 36 (11), 1253–1275. https://doi.org/10.1080/10106049.2019.1641560.
Shahzad, N., Ding, X., Abbas, S., 2022. A comparative assessment of machine learning models for landslide susceptibility mapping in the rugged terrain of Northern Pakistan. Appl. Sci. 12, 2280. https://doi.org/10.3390/app12052280.
Singh, A., Chhetri, N.K., Nitesh Gupta, S.K., Shukla, D.P., 2023. Strategies for sampling pseudo absences of landslide locations for landslide susceptibility mapping in complex mountainous terrain of Northwest Himalaya. Bull. Eng. Geol. Environ. 82, 321. https://doi.org/10.1007/s10064-023-03333-x.
Song, Y., Yang, D., Wu, W., Zhang, X., Zhou, J., Tian, Z., Wang, C., Song, Y., 2023. Evaluating landslide susceptibility using sampling methodology and multiple machine learning models. ISPRS Int. J. Geo Inf. 12 (5), 197. https://doi.org/10.3390/ijgi12050197.
Sun, D., Ding, Y., Zhang, J., Wen, H., Wang, Y., Xu, J., Zhou, X., Liu, R., 2023a. Essential insights into decision mechanism of landslide susceptibility mapping based on different machine learning models. Geocarto Int. 38 (1), 1–29. https://doi.org/10.1080/10106049.2022.2146763.
Sun, D., Chen, D., Zhang, J., Mi, C., Gu, Q., Wen, H., 2023b. Landslide susceptibility mapping based on interpretable machine learning from the perspective of geomorphological differentiation. Land 12, 1018. https://doi.org/10.3390/land12051018.
Tang, L., Yu, X., Jiang, W., Zhou, J., 2023. Comparative study on landslide susceptibility mapping based on unbalanced sample ratio. Sci. Rep. 13, 5823. https://doi.org/10.1038/s41598-023-33186-z.
Thi Ngo, P.T., Panahi, M., Khosravi, K., Ghorbanzadeh, O., Kariminejad, N., Cerda, A., Lee, S., 2021. Evaluation of deep learning algorithms for national scale landslide susceptibility mapping of Iran. Geosci. Front. 12, 505–519. https://doi.org/10.1016/j.gsf.2020.06.013.
Thornthwaite, C.W., 1948. An approach toward a rational classification of climate. Geogr. Rev. 38, 55–94. https://doi.org/10.2307/210739.
Usta, Z., Akıncı, H., Akın, A.T., 2024. Comparison of tree-based ensemble learning algorithms for landslide susceptibility mapping in Murgul (Artvin), Turkey. Earth Sci. Inf. 17, 1459–1481. https://doi.org/10.1007/s12145-024-01259-w.
Üzel Günini, N., Öztürk, D., 2021. Analysis of landslide susceptibility of Van province using frequency ratio method. Uludağ Uni J. Faculty Eng. 26 (3), 865–884. https://doi.org/10.17482/uumfd.969246.
Vakhshoori, V., Pourghasemi, H.R., Zare, M., Blaschke, T., 2019. Landslide susceptibility mapping using GIS-based data mining algorithms. Water 11, 2292. https://doi.org/10.3390/w11112292.
Varnes, D.J., 1978. Slope movement types and processes. In: Schuster, R. L., Krizek, R.J. (Eds.), Landslides Analysis and Control, vol. 176. Transportation Research Board, National Academy of Sciences, New York, NY, USA, pp. 12–33, Special Report.
Vega, J., Sepúlveda-Murillo, F.H., Melissa Parra, M., 2023. Landslide modeling in a tropical mountain basin using machine learning algorithms and shapley additive explanations. Air Soil Water Res. 16, 1–20. https://doi.org/10.1177/11786221231195824.
Wang, Y., Fang, Z., Hong, H., 2019. Comparison of convolutional neural networks for landslide susceptibility mapping in Yanshan County, China. Sci. Total Environ. 666, 975–993. https://doi.org/10.1016/j.scitotenv.2019.02.263.
Wang, Z., Liu, Q., Liu, Y., 2020. Mapping landslide susceptibility using machine learning algorithms and GIS: A case study in Shexian county, Anhui province, China. Symmetry 12, 1954. https://doi.org/10.3390/sym12121954.
Wang, J., Wang, Y., Li, C., Li, Y., Qi, H., 2024. Landslide susceptibility evaluation based on landslide classification and ANN-NFR modelling in the Three Gorges Reservoir area, China. Ecol. Indic. 160, 111920. https://doi.org/10.1016/j.ecolind.2024.111920.
Wei, A., Yu, K., Dai, F., Gu, F., Zhang, W., Liu, Y., 2022. Application of tree-based ensemble models to landslide susceptibility mapping: A comparative study. Sustainability 14, 6330. https://doi.org/10.3390/su14106330.
Wu, Y., Ke, Y., Chen, Z., Liang, S., Zhao, H., Hong, H., 2020. Application of alternating decision tree with AdaBoost and bagging ensembles for landslide susceptibility mapping. Catena 187, 104396. https://doi.org/10.1016/j.catena.2019.104396.
Wubalem, A., 2021. Landslide susceptibility mapping using statistical methods in Uatzau catchment area, northwestern Ethiopia. Geoenviron. Disast. 8, 1. https://doi.org/10.1186/s40677-020-00170-y.
Xiong, H., Ma, C., Li, M., Tan, J., Wang, Y., 2023. Landslide susceptibility prediction considering land use change and human activity: A case study under rapid urban expansion and afforestation in China. Sci. Total Environ. 866, 161430. https://doi.org/10.1016/j.scitotenv.2023.161430.
Xu, K., Zhao, Z., Chen, W., Ma, J., Liu, F., Zhang, Y., Ren, Z., 2024. Comparative study on landslide susceptibility mapping based on different ratios of training samples and testing samples by using RF and FR-RF models. Nat. Hazards Res. 4 (1), 62–74. https://doi.org/10.1016/j.nhres.2023.07.004.
Yalcin, A., Reis, S., Aydinoglu, A.C., Yomralioglu, T., 2011. A GIS-based comparative study of frequency ratio, analytical hierarchy process, bivariate statistics and logistics regression methods for landslide susceptibility mapping in Trabzon, NE Turkey. Catena 85, 274–287. https://doi.org/10.1016/j.catena.2011.01.014.
Yao, Z., Chen, M., Zhan, J., Zhuang, J., Sun, Y., Yu, Q., Yu, Z., 2023. Refined landslide susceptibility mapping by integrating the SHAP-CatBoost

model and InSAR observations: a case study of Lishui, southern China. Appl. Sci. 13, 12817. https://doi.org/10.3390/app132312817.

Yavuz Ozalp, A., Akinci, H., Zeybek, M., 2023. Comparative analysis of tree-based ensemble learning algorithms for landslide susceptibility mapping: a case study in Rize, Turkey. Water 15, 2661. https://doi.org/10.3390/w15142661.

Ye, C., Tang, R., Wei, R., Guo, Z., Zhang, H., 2023. Generating accurate negative samples for landslide susceptibility mapping: A combined self-organizing map and one-class SVM method. Front. Earth Sci. 10, 1054027. https://doi.org/10.3389/feart.2022.1054027.

Ye, P., Yu, B., Chen, W., Liu, K., Ye, L., 2022. Rainfall-induced landslide susceptibility mapping using machine learning algorithms and comparison of their performance in Hilly area of Fujian Province, China. Nat. Hazards 113, 965–995. https://doi.org/10.1007/s11069-022-05332-9.

Yeşilyurt, S.N., Dalkılıç, H.Y., 2021. Daily river flow forecasting with XGBoost and Gradient Boost Machine. The 3rd International Symposium of Engineering Applications on Civil Engineering and Earth Sciences (IEACES2021).

Youssef, A.M., Pourghasemi, H.R., 2021. Landslide susceptibility mapping using machine learning algorithms and comparison of their performance at Abha Basin, Asir Region, Saudi Arabia. Geosci. Front. 12, 639–655. https://doi.org/10.1016/j.gsf.2020.05.010.

Yu, X., Chen, H., 2024. Research on the influence of different sampling resolution and spatial resolution in sampling strategy on landslide susceptibility mapping results. Sci. Rep. 14 (1), 1549. https://doi.org/10.1038/s41598-024-52145-w.

Yu, H., Pei, W., Zhang, J., Chen, G., 2023. Landslide susceptibility mapping and driving mechanisms in a vulnerable region based on multiple machine learning models. Remote Sens. 15, 1886. https://doi.org/10.3390/rs15071886.

Zhang, T., Fu, Q., Li, C., Liu, F., Wang, H., Han, L., Quevedo, R.P., Chen, T., Lei, N., 2022. Modeling landslide susceptibility using data mining techniques of kernel logistic regression, fuzzy unordered rule induction algorithm, SysFor and random forest. Nat. Hazards 114, 3327–3358. https://doi.org/10.1007/s11069-022-05520-7.

Zhang, J., Ma, X., Zhang, J., Sun, D., Zhou, X., Mi, C., Wen, H., 2023. Insights into geospatial heterogeneity of landslide susceptibility based on the SHAP-XGBoost model. J. Environ. Manag. 332, 117357. https://doi.org/10.1016/j.jenvman.2023.117357.

Zhao, X., Chen, W., 2020. Optimization of computational intelligence models for landslide susceptibility evaluation. Remote Sens. 12, 2180. https://doi.org/10.3390/rs12142180.

Zhao, Z., Chen, J., 2023. A robust discretization method of factor screening for landslide susceptibility mapping using convolution neural network, random forest, and logistic regression models. Int. J. Digit. Earth 16 (1), 408–429. https://doi.org/10.1080/17538947.2023.2174192.

Zhou, C., Wang, Y., Cao, Y., Singh, R.P., Ahmed, B., Motagh, M., Wang, Y., Chen, L., Tan, G., Li, S., 2024. Enhancing landslide susceptibility modelling through a novel non-landslide sampling method and ensemble learning technique. Geocarto Int. 39 (1), 2327463. https://doi.org/10.1080/10106049.2024.2327463.